Supplementary Information

Molecular engineering of porphyrin dyes and copper complexes for enhanced dye regeneration toward high-performance dye-sensitized solar cells using copper(I/II) redox shuttles

Yuzhe Zhang,[†] Tomohiro Higashino*,[†] Keigo Namikawa,[†] W. Ryan Osterloh,[†]
and Hiroshi Imahori*,[†,‡,§]

[†] *Department of Molecular Engineering, Graduate School of Engineering, Kyoto University, Nishikyo-ku, Kyoto 615-8510, Japan*

[‡] *Institute for Integrated Cell-Material Science (WPI-iCeMS), Kyoto University, Nishikyo-ku, Kyoto 615-815, Japan*

[§] *Institute for Liberal Arts and Sciences (ILAS), Kyoto University, Kyoto, 606-8316, Japan.*

t-higa@scl.kyoto-u.ac.jp, imahori@scl.kyoto-u.ac.jp

Contents

1. Experimental Section

Instrumentation and Materials.

Commercially available solvents and reagents were used without further purification unless otherwise mentioned. Silica-gel column chromatography was performed with UltraPure Silica Gel (230-400 mesh, SiliCycle) unless otherwise noted. Thin-layer chromatography (TLC) was performed with Silica gel 60 F_{254} (Merck). Size exclusion gel permeation chromatography (GPC) was performed by Bio-beads S-X1 (Bio-rad). UV/Vis/NIR absorption spectra of solutions and films were measured with a Shimadzu UV3600-i Plus spectrometer. Steady-state fluorescence spectra were obtained by a HORIBA Nanolog spectrometer. ^{1}H and ^{13}C NMR spectra were recorded with a JEOL EX-400 spectrometer (operating at 400 MHz for ^{1}H and 100 MHz for ^{13}C) by using the residual solvent as the internal reference for ^{1}H ($CDCl_3$: δ = 7.26 ppm, THF-d_8: 1.72 and 3.58 ppm) and ^{13}C ($CDCl_3$: δ = 77.16 ppm, THF-d_8: 67.21 and 25.31 ppm). High-resolution mass spectra (HR-MS) were measured on a Thermo Fischer Scientific EXACTIVE spectrometer for APCI and ESI measurements. Elemental analysis data were obtained *via* Center for Organic Elemental Microanalysis, Kyoto University. Attenuated total reflectance-Fourier transform infrared (ATR-FTIR) spectra were recorded on a NICOLET iS50 spectrometer. Electrical impedance spectra were measured on SP-150 (Bio-Logic) spectrometer.

Electrochemical Measurements.

Electrochemical measurements were made using an ALS electrochemical analyzer model 601E with DPV technique. Redox potentials were determined by differential pulse voltammetry (DPV) in THF containing 0.1 M tetrabutylammonium hexafluorophosphate (n-Bu_4NPF_6). A glassy carbon (3 mm diameter) working electrode, Ag/Ag^+ (sat. KCl) reference electrode, and Pt wire counter electrode were employed. Ferrocene (+0.642 V vs NHE) was used as an internal standard.

For determination of diffusion coefficients (D), a three-electrode cell consisting of a glassy carbon (3 mm diameter) working electrode, Ag/Ag^+ (sat. KCl) reference electrode, and Pt wire counter electrode, was used to perform the chronoamperometric experiments. The current-time curves were recorded and a plot of $it^{1/2}$ *vs.* $t^{1/2}$ were used to extrapolate the D according to the following equation[S1]:

$$D^{1/2} = \frac{(it^{1/2})_{t=0\pi^{1/2}}}{nFAC}$$

where D is the diffusion coefficient, i is the current, t is the time, n is the number of electrons, F is faraday constant, A is the electrode area, and C is the bulk concentration of electroactive species. It should be noted that the background current was negligible and the exact area of the working electrode (A = X cm^{-2}) was determined by measuring the diffusion coefficient of Ferrocene in CH_3CN/n-Bu_4NPF_6 ($D = 2.24 \times 10^{-5}$ cm^2).

Bulk electrolysis of copper(I) complexes to copper(II) complexes

Bulk electrolysis experiments were performed in a conventional three-electrode cell equipped with a large-area platinum mesh working electrode, a platinum wire counter electrode, and an Ag/Ag$^+$ (sat. KCl) reference electrode. The electrochemical cell is divided into two compartments by a fritted glass separator (pore size: 16–40 μm). The electrochemical cell was connected to an electrochemical workstation (ALS electrochemical analyzer model 601E with DPV technique). A solution of **[Cu(2MeOby)$_2$][X]** (X = TFSI, BF_4, or PF_6) (1-5 mM) was prepared in anhydrous acetonitrile containing 0.1 M LiX (X = TFSI, BF_4, or PF_6) as the supporting electrolyte. Prior to electrolysis, the solution was purged with high-purity argon gas for 15 minutes to remove dissolved oxygen. Bulk electrolysis was carried out under an applied potential of +1.0 V *vs.* Ag/Ag$^+$ (sat. KCl) at room temperature with continuous magnetic stirring (Figure S16). The progress of electrolysis was monitored by recording the current, and the electrolysis was continued until the current decayed to a negligible value (<0.5% relative to the initial current), indicating the complete conversion of the copper(I) complex to the corresponding copper(II) species (Figure S17). The resulting solution containing the electrochemically generated **[Cu(2MeOby)$_2$][X]$_2$** (X = TFSI, BF_4, or PF_6) was immediately transferred to a quartz cuvette for UV/vis/NIR absorption and CV/DPV measurements (Figures S18 and S19). Assuming that the concentrations of the copper species are identical during the electrolysis and the supporting electrolytes (LiX; X = TFSI, BF_4, or PF_6) have negligible influence on the optical properties, we determined the molar absorption coefficients of the copper(II) complexes from the absorbances of the resulting solution.

Density Functional Theory (DFT) Calculations.

All calculations were carried out using the *Gaussian 09* program.[S2] All structures of porphyrins were fully optimized without any symmetry restriction. The calculations were performed by the density functional theory (DFT) method with restricted B3LYP (Becke's three-parameter hybrid exchange functionals and the Lee-Yang-Parr correlation functional) level, employing a basis set 6-31G(d) for C, H, N, O, S, and Zn.

Preparation of Porphyrin-Sensitized TiO_2 Electrode and Photovoltaic Measurements.

The preparation of TiO_2 electrodes and the fabrication of the sealed cells for photovoltaic measurements were performed according to literature.[S3,S4] We used two types of TiO_2 pastes, one composed of nanocrystalline TiO_2 particles (30 nm, PST30NR-D, GreatCell Solar) and another containing submicrocrystalline TiO_2 particles (400 nm, CCIC:PST400C, JGC-C&C), to form the transparent and the light-scattering layers of the photoanode, respectively. To prepare the working electrodes, FTO glasses (solar 4 mm thickness, 10 Ω/sq, Nippon Sheet Glass) were first cleaned in a hydrochloric acid aqueous solution (0.1 M) using an ultrasonic bath for 15 min and then rinsed with distilled water and ethanol. After UV-O_3 irradiation for 18 min, the FTO glass plates were immersed into a 40 mM aqueous $TiCl_4$ solution at 70 °C for 30 min and washed with distilled water. A nanocrystalline TiO_2 layer of 2 μm (for copper complex-based redox shuttles) or 8 μm (for I^-/I_3^- redox shuttle) was coated on the FTO glass plate by a screen-printing method, kept in a clean box for 4 minutes, and then dried over 6 min at 125 °C. After drying the films at 125 °C, a layer of the submicrocrystalline TiO_2 paste was further deposited twice by screen-printing in the same method as the fabrication of the nanocrystalline TiO_2 layer, resulting in formation of a light-scattering TiO_2 film of 4 μm on the transparent TiO_2 film. Finally, the electrodes coated with the TiO_2 pastes were gradually heated under an airflow at 325 °C for 5 min, at 375 °C for 5 min, at 450 °C for 15 min, and at 500 °C for 15 min. The thickness of the films was determined using a surface profiler (DektakXT, Bruker). The size of the TiO_2 film was 0.14 cm^2 (3.8 × 3.8 mm). The TiO_2 electrode was treated again with 40 mM $TiCl_4$ solution at 70 °C for 25 min and then rinsed with distilled water, sintered at 550 °C for 30 min, and cooled to 110 °C before dipping into the dye solution. For **FL1**, the TiO_2 electrode was immersed into a toluene and ethanol solution (v/v = 1/5) of the porphyrin dye (0.20 mM) in the presence of chenodeoxycholic acid (CDCA, 1 equiv.) at 25 °C for 3 h. For **LG4**, the TiO_2 electrode was immersed into an acetonitrile and *tert*-butyl alcohol (v/v = 1/1) solution of the porphyrin dye (0.20 mM) in the presence of CDCA (4 equiv.) at 25 °C for 3h. For co-sensitization with **XY1B**, the TiO_2 electrode was firstly immersed into the porphyrin dye solution (0.20 mM) under the optimized conditions (solvent and concentration of CDCA) at 25 °C for 3 h, washed with acetonitrile, dried in air, and then immersed into a THF and ethanol solution (v/v = 1/4) of **XY1B** (0.10 mM, with 50 equivalent of CDCA) at 25 °C for 2 h. The surface coverage of the dyes on TiO_2 film (Γ, mol cm^{-2}) were determined by measuring the absorbance of the dyes that were detached from the dye-stained TiO_2 film into 0.1 M NaOH solution of 1:1 mixture of THF and water.

The counter electrode was prepared by drilling a small hole in an FTO glass (1.6 mm thickness, 10 Ω/sq, Nippon Sheet Glass), rinsing with distilled water and ethanol followed by treatment with 0.1 M HCl solution in 2-propanol using an ultrasonic bath for 15 min. Then the platinum was deposited on the FTO glass by coating with a drop of H_2PtCl_6 solution (2 mg in 1 mL of ethanol) once. Finally, the FTO glass was heated at 400 °C for 15 min to obtain the counter Pt-electrode.

A sandwich cell was prepared by using the dye-anchored TiO_2 film as a working electrode and a counter Pt-electrode, which were assembled with a hotmelt-ionomer film Surlyn polymer gasket (DuPont, 25 μm), and the superimposed electrodes were tightly held and heated at 140 °C to seal the two electrodes. The aperture of the Surlyn frame was 2 mm larger than that of the area of the TiO_2 film, and its width was 1 mm. The hole in the counter Pt-electrode was sealed by a film of Surlyn. A hole was then made in the film of Surlyn covering the hole with a needle. A drop of an electrolyte was put on the hole in the back of the counter Pt-electrode. It was introduced into the cell via vacuum backfilling. Finally, the hole was sealed using Surlyn film and a cover glass (0.13–0.17 mm thickness). A solder was applied on each edge of the FTO electrodes.

The electrolyte solutions containing copper complex-based redox shuttles with the accurate concentrations were prepared by adjusting the amounts of copper(I/II) complexes based on the actual composition of the copper(II) complex **$[Cu(L)_2][X]_n$** (n = 1.6–1.9; L = **tmby** or **2MeOby**; X = TFSI, BF_4, or PF_6). The copper-based electrolyte with high concentration was composed of 0.20 M **$[CuL_2][TFSI]$**, 0.05 M **$[CuL_2][TFSI]_2$**, 0.1 M lithium salt (LiTFSI), and 0.5 M 4-*tert*-butylpyridine (TBP) in acetonitrile (L = **tmby** or **2MeOby**). The copper-based electrolyte with low concentration was composed of 0.10 M **$[CuL_2][X]$**, 0.025 M **$[CuL_2][X]_2$**, 0.1 M lithium salt (LiX), and 0.5 M TBP in acetonitrile (L = **tmby** or **2MeOby**; X = TFSI, BF_4, or PF_6). The iodine-based electrolyte was composed of 0.6 M dimethylpropyl-imidazolium iodide, 0.05 M I_2, 0.1 M LiI, and 0.5 M TBP in acetonitrile.

Incident photon-to-current efficiency (IPCE) and photocurrent-voltage (*I-V*) performance were measured on an action spectrum measurement setup (CEP-2000RR, BUNKOUKEIKI) and a solar simulator (PEC-L10, Peccell Technologies) with a simulated sunlight of AM 1.5 (100 mW cm^{-2}), respectively: IPCE (%) = 100 × 1240 × $i/(W_{in} \times \lambda)$, where i is the photocurrent density (A cm^{-2}) W_{in} is the incident light intensity (W cm^{-2}), and λ is the excitation wavelength (nm). During the photovoltaic measurements, the cells with a photoactive area of 0.14 cm^2 were covered with a black mask with an aperture area of 0.086 cm^2 to avoid scattering light. The convolution of the spectral response in the photocurrent action spectrum with the photon flux of the AM 1.5G spectrum provided the estimated J_{SC}-value, which is lower than the J_{SC}-value obtained from the *I-V* performance due to the low stability of the DSSCs.

Time-resolved Transient Absorption Spectroscopy.

The measurements were carried out with the laser system provided by UNISOKU according to the following procedure: A sample was excited by a Panther optical parametric oscillator pumped by a Nd:YAG laser (Continuum, Surelite SLI-10; 4–6 ns FWHM) at λ = 540 nm. The photodynamics was monitored by continuous exposure to a Xe lamp as a probe light and a photomultiplier tube (Unisoku, NIR-PD1) as a detector. The output from the photodiodes and a photomultiplier tube was recorded with a digitizing oscilloscope (Iwatsu, Digital Oscilloscope DS-5532). All the samples were made by the same method for preparing the porphyrin on the TiO_2 electrodes (*vide supra*).

2. Synthesis

2-Bromo-9,9′-dioctyl-9*H*-fluorene (**1**),[S5] compound **3**,[S6] **LG4**,[S7] 4,4′,6,6′-tetramethyl-2,2′-bipyridine (**tmby**),[S8] 4,4′-dimethoxy-6,6′-dimethyl-2,2′-bipyridine (**2MeOby**),[S9] **[Cu(tmby)$_2$][TFSI]**,[S10] and **[Cu(tmby)$_2$][TFSI]$_2$**[S10,S11] were prepared according to the literatures.

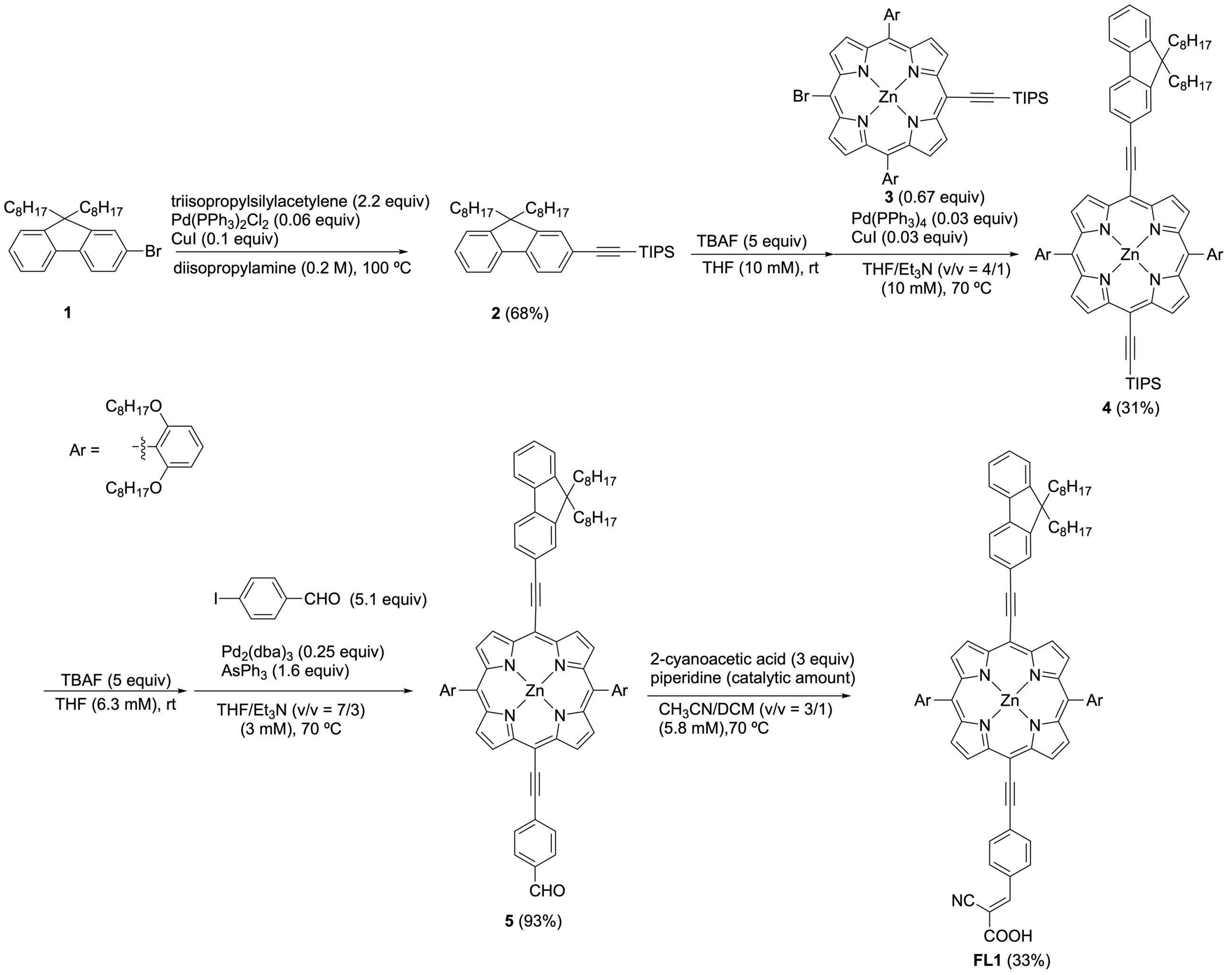

Scheme S1. Synthesis of porphyrin **FL1**.

Compound 2: 2-Bromo-9,9′-dioctyl-9*H*-fluorene (**1**) (131 mg, 0.28 mmol, 1.0 equiv.), Pd(PPh$_3$)$_2$Cl$_2$ (12 mg, 0.017 mmol, 0.061 equiv.) and CuI (5.0 mg, 0.028 mmol, 0.10 equiv.) were added to diisopropylamine (1.2 mL) in a Schlenk tube. Then triisopropylsilylacetylene (0.14 mL, 0.62 mmol, 2.2 equiv.) was added dropwise to the mixture. The reaction mixture was heated to 100 °C with stirring for 15 h under argon. The mixture was cooled to room temperature, washed with water, extracted with AcOEt and the organic layer was dried over anhydrous Na$_2$SO$_4$. After the solvent was removed, the crude product was purified by column chromatography on silica gel using hexane and GPC using CHCl$_3$ as eluent to compound **2** as a colorless oil (106 mg, 0.19 mmol, 68%).

^{1}H NMR (CDCl$_3$, 400 MHz): δ = 7.69 (dd, J = 7.8 Hz, J = 1.8 Hz, 1H, Ar-H), 7.63 (d, J = 7.8 Hz, 1H, Ar-H), 7.48 (dd, J = 7.8 Hz, J = 1.4 Hz, 1H, Ar-H), 7.43 (s, 1H, Ar-H), 7.33 (m, 3H, Ar-H), 1.97 (t, J = 8.7 Hz, 4H, $CH_2C_6H_{12}CH_3$), 1.19–0.86 (m, 45H, TIPS and $CH_2C_6H_{12}CH_3$), and 0.84 (t, *J* = 7.3 Hz, 6H, $CH_2C_6H_{12}CH_3$) ppm. ^{13}C NMR ($CDCl_3$, 100 MHz): δ = 151.2, 150.8, 141.6, 140.6, 131.5, 127.6, 127.0, 126.2, 123.0, 120.1, 121.9, 119.5, 108.4, 90.2, 55.2, 40.4, 31.9, 30.1, 29.4, 29.3, 23.8, 22.8, 18.9, 14.2, and 11.6 ppm. HRMS (APCI) calcd for $C_{40}H_{62}Si_1$ [*M*+H]$^+$: 571.4694; found 571.4691. FTIR (ATR): ν = 2924, 2856, 2149, 1464, 1451, 1415, 1379, 1267, 1155, 1072, 1016, 995, 918, 882, 830, 780, 738, 675, and 635 cm^{-1}.

Due to the very complicated signals, we cannot provide the complete assignments of the ^{13}C NMR signals.

Porphyrin 4: A 1.0 M solution of TBAF in THF (1.9 mL, 1.9 mmol, 7.5 equiv.) was added dropwise to a solution of compound **2** (211 mg, 0.37 mmol, 1.5 equiv.) in dry THF (37 mL). The solution was stirred at room temperature for 2 h under argon. The mixture was quenched with water and then extracted with CH_2Cl_2. The organic layer was dried over anhydrous Na_2SO_4 and the solvent was removed. The residue was dissolved in dry THF (10mL) and added to the solution of dry THF (25 mL), NEt_3 (5.7 mL), porphyrin **3** (316 mg, 0.24 mmol, 1.0 equiv.), $Pd(PPh_3)_4$ (14 mg, 0.012 mmol, 0.050 equiv.) and CuI (2.0 mg, 0.012 mmol, 0.050 equiv.). The solution was heated to 70 °C and stirred for 21 h under argon. The mixture was cooled to room temperature, washed with water, extracted with CH_2Cl_2, and the organic layer was dried over anhydrous Na_2SO_4. The solvent was removed under reduced pressure and the crude product was purified by column chromatography on silica gel using CH_2Cl_2 and hexane (v/v = 3/7) as eluent to give porphyrin **4** as green solid (206 mg, 0.13 mmol, 31%).

^{1}H NMR ($CDCl_3$, 400 MHz): δ = 9.76 (d, *J* = 4.6 Hz, 2H, β), 9.67 (d, *J* = 4.1 Hz, 2H, β), 8.90 (d, *J* = 4.1 Hz, 2H, β), 8.86 (d, *J* = 4.6 Hz, 2H, β), 8.03 (d, *J* = 7.8 Hz, 1H, Ar-H), 7.97 (s, 1H, Ar-H), 7.89 (d, *J* = 7.8 Hz, 1H, Ar-H), 7.82 (d, *J* =6.4 Hz, 1H, Ar-H), 7.71 (t, *J* =8.2 Hz, 2H, Ar-H), 7.40 (m, 3H, Ar-H), 7.02 (d, *J* = 8.7 Hz, 4H, Ar-H), 3.86 (t, *J* = 6.4 Hz, 8H, $OCH_2C_7H_{15}$), 2.16 (m, 4H, $CH_2C_6H_{12}CH_3$), 1.47 (s, 21H, TIPS), 1.23–1.48 (m, 20H), 1.00–0.80 (m, 24H) and 0.72–0.46 (m, 46H) ppm. ^{13}C NMR ($CDCl_3$, 100 MHz): δ = 160.1, 152.3, 151.6, 151.3, 151.2, 150.75, 150.65, 141.4, 140.9, 131.9, 131.8, 130.8, 130.7, 130.6, 129.8, 127.6, 127.1, 125.8, 123.12, 123.10, 121.3, 120.1, 120.0, 115.2, 110.5, 105.3, 100.5, 100.1, 96.8, 96.4, 93.8, 68.8, 64.9, 55.4, 40.7, 32.0, 31.5, 30.3, 29.4, 28.8, 25.4, 24.0, 23.4, 22.7, 22.4, 19.3, 19.2, 14.2, 14.0, and 12.1 ppm. HRMS (APCI) calcd for $C_{106}H_{144}N_4O_4Si_1Zn_1$ [*M*+H]$^+$: 1630.0321; found 1630.0282. FTIR (ATR): ν = 2923, 2853, 2136, 1586, 1501, 1454, 1378, 1338, 1302, 1246, 1209, 1123, 1097, 1059, 998, 883, 826, 794, 768, 710, and 655 cm^{-1}. m.p.: 60-61 °C.

Due to the very complicated signals, we cannot provide the complete assignments of the ^{13}C NMR signals.

Porphyrin 5: A 1.0 M solution of TBAF in THF (0.45 mL, 0.45 mmol, 5.1 equiv.) was added dropwise to a solution of porphyrin **4** (146 mg, 0.089 mmol, 1.0 equiv.) in dry THF (14 mL). The solution was stirred at room temperature for 1 h under argon. The mixture was quenched with water and then extracted with CH_2Cl_2. The organic layer was dried over anhydrous Na_2SO_4 and the solvent was removed. The residue was dissolved in dry THF (16 mL) and NEt_3 (6.1 mL). 4-iodobenzaldehyde (105 mg, 0.45 mmol, 5.1 equiv.), $Pd_2(dba)_3$ (20.0 mg, 0.022 mmol, 0.25 equiv.) and $AsPh_3$ (43.0 mg, 0.14 mmol, 1.6 equiv.) were added to the mixture. The solution was heated to 70 °C and stirred for 2.5 h under argon. The mixture was cooled to room temperature, washed with water, extracted with CH_2Cl_2, and the organic layer was dried over anhydrous Na_2SO_4. The solvent was removed under reduce pressure and the crude product was purified by column chromatography on silica gel using CH_2Cl_2/hexane (v/v = 3/7) and GPC as eluent to give porphyrin **5** as green solid (131 mg, 0.083 mmol, 93%).

^{1}H NMR ($CDCl_3$, 400 MHz): δ = 9.82 (s, 1H, CHO), 9.78 (d, J = 4.6 Hz, 2H, β), 9.62 (d, J = 4.6 Hz, 2H, β), 8.93 (d, J = 4.6 Hz, 4H, β), 8.01 (dd, J = 7.8, 1.4 Hz, 1H, Ar-H), 7.96 (s, 1H, Ar-H), 7.89 (d, J = 7.8 Hz, 1H, Ar-H), 7.82 (m, 3H, Ar-H), 7.74 (m, 4H, Ar-H), 7.40 (m, 3H, Ar-H), 7.04 (d, J = 8.7 Hz, 4H, Ar-H), 3.89 (t, J = 6.4 Hz, 8H, $OC\mathit{H}_2C_7H_{15}$), 2.13 (m, 4H, $C\mathit{H}_2C_6H_{12}CH_3$), 1.22-1.13 (m, 20H), 1.05-0.98 (m, 8H), 0.85-0.76 (m, 16H), and 0.65-0.41 (m, 46H) ppm. ^{13}C NMR ($CDCl_3$, 100 MHz): δ = 191.3, 160.0, 151.9, 151.7, 151.3, 151.2, 150.9, 150.8, 141.6, 140.8, 134.9, 132.4, 132.1, 131.6, 131.0, 130.8, 130.7, 130.5, 130.1, 129.7, 128.7, 127.7, 127.1, 125.9, 123.1, 122.8, 120.7, 120.2, 120.0, 115.9, 105.3, 101.7, 98.9, 97.9, 97.5, 94.9, 93.1, 68.8, 55.4, 40.7, 32.0, 31.5, 30.3, 29.4, 28.77, 28.75, 28.7, 25.4, 24.0, 22.8, 22.4, 14.2, and 14.0 ppm. HRMS (APCI) calcd for $C_{104}H_{128}N_4O_5Zn_1$ $[M+H]^+$: 1577.9249; found 1577.9214. FTIR (ATR): ν = 2921, 2851, 2187, 1670, 1595, 1557, 1505, 1453, 1377, 1245, 1204, 1163, 1095, 1059, 998, 943, 826, 793, 769, 720, and 710 cm^{-1}. m.p.: 91-92 °C.

Due to the very complicated signals, we cannot provide the complete assignments of the ^{13}C NMR signals.

FL1: A mixture of porphyrin **5** (131 mg, 0.083 mmol, 1.0 equiv.), 2-cyanoacetic acid (21.0 mg, 0.25 mmol, 3.0 equiv.) and piperidine (two drops) in CH_3CN (10.7 mL) and $CHCl_3$ (3.60 mL) was stirred for 15 h at 70 °C under argon. The mixture was cooled to room temperature, washed with HCl aq. (0.1 M) and water, extracted with CH_2Cl_2, and the organic layer was dried over anhydrous Na_2SO_4. The solvent was removed under reduce pressure and the crude product was purified by column chromatography on silica gel using CH_2Cl_2 and CH_2Cl_2/MeOH (v/v = 20/1), and GPC using THF as eluent to give **FL1** as green solid (45.0 mg, 0.027 mmol, 33%).

^{1}H NMR (THF-d_8, 400 MHz): δ = 10.84 (s, 1H, COOH), 9.64 (d, J = 4.6 Hz, 2H, β), 9.60 (d, J = 4.6 Hz, 2H, β), 8.77 (q, J = 4.4 Hz, 4H, β), 8.36 (s, 1H, alkynyl), 8.29 (d, J = 8.2 Hz, 2H, Ar-H), 8.17 (d, J = 8.2 Hz, 2H, Ar-H), 8.02 (m, 2H, Ar-H), 7.94 (d, J = 7.8 Hz, 1H, Ar-H), 7.84 (dd, J = 6.2, 2.1 Hz, 1H, Ar-H), 7.71 (t, J = 8.5 Hz, 2H, Ar-H), 7.45 (s, 1H, Ar-H), 7.37-7.34 (m, 2H, Ar-H), 7.08 (d, J = 8.2 Hz, 4H, Ar-H), 3.90 (t, J = 6.6 Hz, 8H, $OC\mathit{H}_2C_7H_{15}$), 2.23-2.14 (m, 4H, $C\mathit{H}_2C_6H_{12}CH_3$), 1.34-1.13 (m, 25H), and 0.99-0.60 (m, 72H). ^{13}C NMR(THF-d_8, 100 MHz): δ = 160.8, 152.3, 151.9, 151.7, 151.6, 151.5, 151.3, 150.4, 142.2, 132.4, 132.3, 132.0, 131.9, 131.2, 130.7, 130.5, 130.3, 126.2, 125.7, 124.0, 123.5, 121.5, 120.7, 120.6, 116.3, 105.3, 101.3, 99.6, 98.5, 94.7, 79.3, 68.9, 66.1, 55.9, 54.7, 41.2, 34.9, 32.6, 32.34, 32.29, 30.9, 30.6, 30.5, 30.2, 30.1, 30.0, 29.65, 29.58, 29.55, 26.1, 23.34, 23.28, 23.1, 15.5, 14.2, and 14.1 ppm. HRMS (APCI, CH_2Cl_2 solution) calcd for $C_{107}H_{129}N_5O_6ZnCl$ [*M*+Cl]$^-$: 1678.8928; found 1678.8957. Elemental analysis: calcd. for $C_{107}H_{129}N_5O_6Zn$: C 78.05, H 7.9, N 4.25; found C 76.8, H 7.8, N 4.0. FTIR (ATR): ν = 3320, 2922, 2851, 2227, 2184, 1694, 1578, 1505, 1453, 1377, 1339, 1246, 1205, 1183, 1093, 1060, 997, 942, 830, 791, 769, 721, and 709 cm^{-1}. m.p.: 240-241 °C.

Due to the very complicated signals, we cannot provide the complete assignments of the ^{13}C NMR signals.

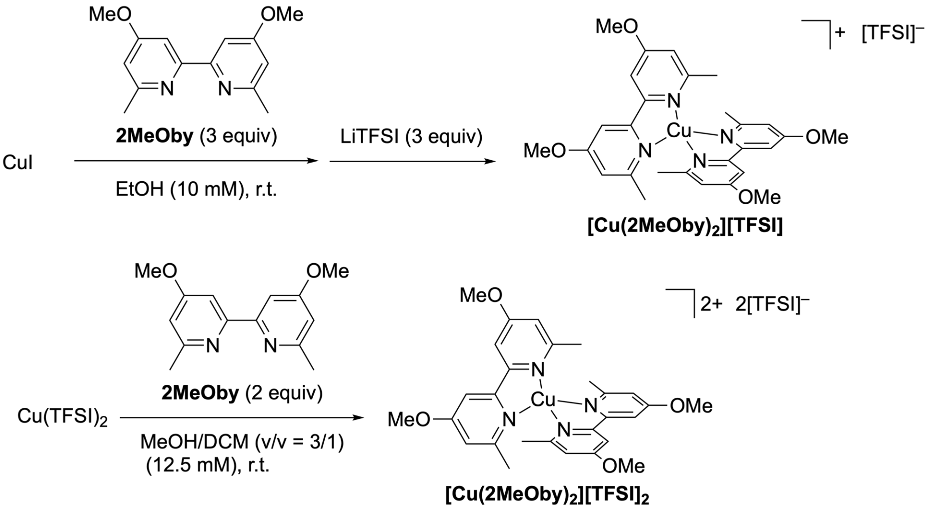

Scheme S2. Synthesis of **[Cu(2MeOby)$_2$][TFSI]** and **[Cu(2MeOby)$_2$][TFSI]$_2$**.

[Cu(2MeOby)$_2$][TFSI]: A mixture of CuI (76 mg, 0.40 mmol, 1.0 equiv.) and **2MeOby** (292 mg, 1.2 mmol, 3.0 equiv.) in ethanol (40 mL) was stirred for 1 h at room temperature under argon atmosphere. Then, LiTFSI (344 mg, 1.2 mmol, 3.0 equiv.) was added and the mixture was stirred for 2 h. A red solid was collected by filtration and washed with ethanol to give the **[Cu(2MeOby)$_2$][TFSI]** (310 mg, 0.37 mmol, 93%).

^{1}H NMR ($CDCl_3$, 400 MHz): δ = 7.52 (d, *J* = 2.3 Hz, 2H, Ar-H), 6.90 (d, *J* = 1.8 Hz, 2H, Ar-H), 4.00 (s, 6H, OCH_3), and 2.19 (s, 6H, CH_3) ppm. ^{13}C NMR ($CDCl_3$, 100 MHz): δ = 167.3 (pyridyl-2C), 158.8 (pyridyl-4C), 153.3 (pyridyl-6C), 110.7 (pyridyl-5C), 106.3 (pyridyl-3C), 56.2 ($-OCH_3$), and 25.4 ($-CH_3$) ppm. ESI-MS (positive): *m*/*z* calcd. for $C_{28}H_{32}CuN_4O_4$ [*M*–TFSI]$^+$: 551.1714; found 551.1700. ESI-MS (negative): *m*/*z* calcd. for $C_2F_6NO_4S_2$ [TFSI]$^-$: 279.9178; found 279.9179. Elemental analysis: calcd. for $C_{30}H_{32}CuF_6N_5O_8S_2$: C 43.3, H 3.9, N 8.4; found C 43.1, H 4.0, N 8.4. m.p.: 201 °C.

[Cu(2MeOby)$_2$][TFSI]$_2$: A mixture of Cu(TFSI)$_2$ (156 mg, 0.25 mmol, 1.0 equiv.) and **2MeOby** (122 mg, 0.50 mmol, 2.0 equiv.) in MeOH/dichloromethane (v/v = 3/1, 20 mL) was stirred for 2 h at room temperature under argon atmosphere. The solvent was evaporated, and the residue was re-dissolved in dichloromethane (5.0 mL). Then, Et_2O was added to the solution to form the precipitate. The precipitate was collected by filtration and the resultant brown solid was washed with ethanol and

Et_2O to give the copper(II) complex (110 mg) as a mixture of **[Cu(2MeOby)$_2$][TFSI]$_2$** and **[Cu(2MeOby)$_2$][TFSI].** The actual composition of the as-prepared copper (II) complex was determined to be **[Cu(2MeOby)$_2$][TFSI]$_{1.6}$** from the absorbance at 748 nm in acetonitrile.
Elemental analysis: calcd. for $C_{31.2}H_{32}CuF_{9.6}N_{5.6}O_{10.4}S_{3.2}$: C 37.5, H 3.2, N 7.8; found C 37.3, H 3.2, N7.75.

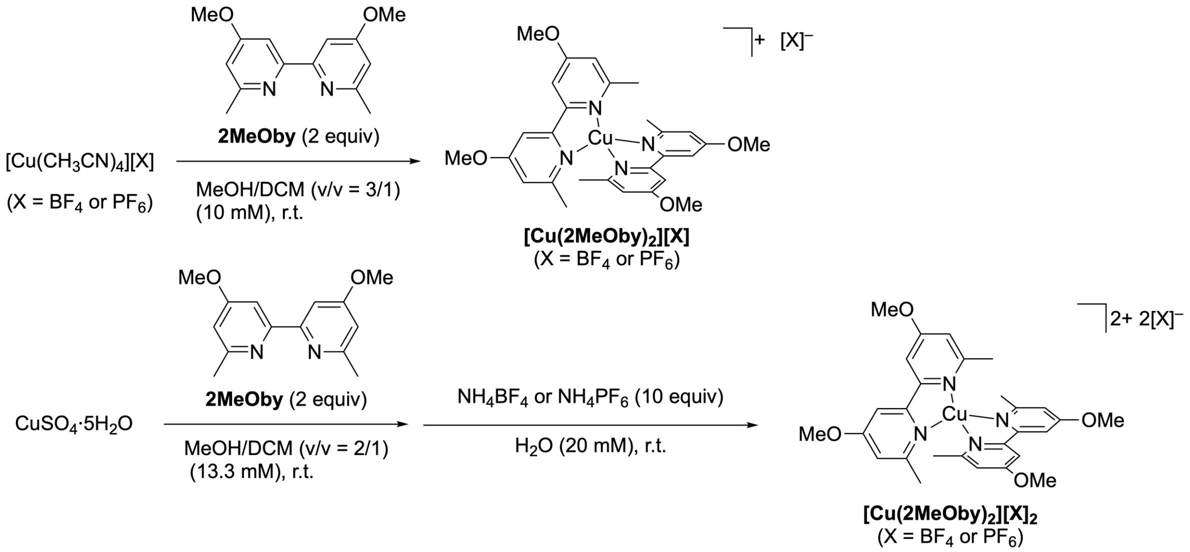

Scheme S3. Synthesis of **[Cu(2MeOby)$_2$][X]** and **[Cu(2MeOby)$_2$][X]$_2$** (X = BF_4 or PF_6).

[Cu(2MeOby)$_2$][BF$_4$]: A mixture of [Cu(CH_3CN)$_4$][BF_4] (94 mg, 0.30 mmol, 1.0 equiv.) and **2MeOby** (147 mg, 0.60 mmol, 2.0 equiv.) in dichloromethane/MeOH (v/v = 3/1, 30 mL) was stirred for 2 h at room temperature under argon atmosphere. The solvent was evaporated, and the residue was re-dissolved in dichloromethane (6.0 mL). Then, Et_2O was added to the solution to form the precipitate. A red solid was collected by filtration, and washing by EtOH and Et_2O to give **[Cu(2MeOby)$_2$][BF$_4$]** (135 mg, 0.21 mmol, 70%).
^{1}H NMR ($CDCl_3$, 400 MHz): δ = 7.66 (d, J = 1.8 Hz, 2H, Ar-H), 6.89 (d, J = 1.8 Hz, 2H, Ar-H), 4.05 (s, 6H, OCH_3), and 2.18 (s, 6H, CH_3) ppm. ^{13}C NMR ($CDCl_3$, 100 MHz): δ = 167.4 (pyridyl-2C), 158.5 (pyridyl-4C), 153.6 (pyridyl-6C), 111.3 (pyridyl-5C), 106.0 (pyridyl-3C), 56.5 (-OCH_3), and 25.3 (-CH_3) ppm. ESI-MS (positive): m/z calcd. for $C_{28}H_{32}CuN_4O_4$ $[M–BF_4]^+$: 551.1714; found 551.1711. ESI-MS (negative): m/z calcd. BF_4 $[BF_4]^-$: 87.0035; found 87.0029. Elemental analysis: calcd. for $C_{28}H_{32}BCuF_4N_4O_4$: C 52.6, H 5.05, N 8.8; found C 52.4, H 5.0, N 8.8. m.p.: 286 °C.

[Cu(2MeOby)$_2$][BF$_4$]$_2$: A mixture of $CuSO_4·5H_2O$ (25 mg, 0.10 mmol, 1.0 equiv.) and **2MeOby** (49 mg, 0.30 mmol, 2.0 equiv.) in MeOH/dichloromethane (v/v = 2/1, 7.5 mL) was stirred for 2 h at room temperature under argon atmosphere. The solvent was evaporated, and the residue was re-dissolved in distilled water (5.0 mL). Then, the aqueous solution (5.0 mL) of NH_4BF_4 (105 mg, 1.0 mmol, 10 equiv.) was slowly added dropwise to the solution. The precipitate was collected by filtration and the recrystallization by dichloromethane/Et_2O afforded the copper(II) complex (30 mg) as a mixture of **[Cu(2MeOby)$_2$][BF$_4$]$_2$** and **[Cu(2MeOby)$_2$][BF$_4$]**. The actual composition of the as-prepared copper(II) complex was determined to be **$[Cu(2MeOby)_2][BF_4]_{1.9}$** from the absorbance at 748 nm in acetonitrile. Elemental analysis: calcd. for $C_{28}H_{32}B_{1.9}CuF_{7.6}N_4O_4$: C 46.9, H 4.5, N 7.8; found C 44.8, H 4.5, N 7.5.

$[Cu(2MeOby)_2][PF_6]$: A mixture of $[Cu(CH_3CN)_4][PF_6]$ (112 mg, 0.30 mmol, 1.0 equiv.) and **2MeOby** (147 mg, 0.60 mmol, 2.0 equiv.) in dichloromethane/MeOH (v/v = 3/1, 30 mL) was stirred for 2 h at room temperature under argon atmosphere. The solvent was evaporated, and the residue was re-dissolved in dichloromethane (6.0 mL). Then, Et_2O was added to the solution to form the precipitate. A red solid was collected by filtration, and washing by EtOH and Et_2O to give **$[Cu(2MeOby)_2][PF_6]$** (130 mg, 0.19 mmol, 62%).

^1H NMR ($CDCl_3$, 400 MHz): $\delta = 7.54$ (s, 2H, Ar-H), 6.90 (s, 2H, Ar-H), 4.02 (s, 6H, OC*H*3), and 2.18 (s, 6H, C*H*3) ppm. ^{13}C NMR ($CDCl_3$, 100 MHz): $\delta = 167.3$ (pyridyl-2C), 158.7 (pyridyl-4C), 153.4 (pyridyl-6C), 111.0 (pyridyl-5C), 106.0 (pyridyl-3C), 56.3 ($-OCH_3$), and 25.4 ($-CH_3$) ppm. ESI-MS (positive): *m*/*z* calcd. for $C_{28}H_{32}CuN_4O_4$ $[M-PF_6]^+$: 551.1714; found 551.1710. ESI-MS (negative): *m*/*z* calcd. FP_6 $[PF_6]^-$: 144.9647; found 144.9649. Elemental analysis: calcd. for $C_{28}H_{32}CuF_6N_4O_4P$: C 48.2, H 4.6, N 8.0; found C 48.0, H 4.5, N 7.9. m.p.: 261 °C.

$[Cu(2MeOby)_2][PF_6]_2$: A mixture of $CuSO_4{\cdot}5H_2O$ (50 mg, 0.20 mmol, 1.0 equiv.) and **2MeOby** (97 mg, 0.40 mmol, 2.0 equiv.) in MeOH/dichloromethane (v/v = 2/1, 15 mL) was stirred for 2 h at room temperature under argon atmosphere. The solvent was evaporated, and the residue was re-dissolved in distilled water (10 mL). Then, the aqueous solution (10 mL) of NH_4PF_6 (326 mg, 2.0 mmol, 10 equiv.) was slowly added dropwise to the solution. The precipitate was collected by filtration and the recrystallization by dichloromethane/Et_2O afforded the copper(II) complex (55 mg) as a mixture of **$[Cu(2MeOby)_2][PF_6]_2$** and **$[Cu(2MeOby)_2][PF_6]$**. The actual composition of the as-prepared copper(II) complex was determined to be **$[Cu(2MeOby)_2][PF_6]_{1.9}$** from the absorbance at 748 nm in acetonitrile. Elemental analysis: calcd. for $C_{28}H_{32}CuF_{11.4}N_4O_4P_{1.9}$: C 40.6, H 3.9, N 6.8; found C 40.4, H 3.8, N 6.6.

$[Cu(tmby)_2][TFSI]_2$: We prepared **$[Cu(tmby)_2][TFSI]_2$** according to the literature[S10,S11] and obtained the solid as a mixture of **$[Cu(tmby)_2][TFSI]_2$** and **$[Cu(tmby)_2][TFSI]$**.[S13] The actual composition of the as-prepared copper(II) complex should be determined to be **$[Cu(tmby)_2][TFSI]_{1.8}$** from the absorbance at 730 nm in acetonitrile.

3. High-Resolution Mass Spectra

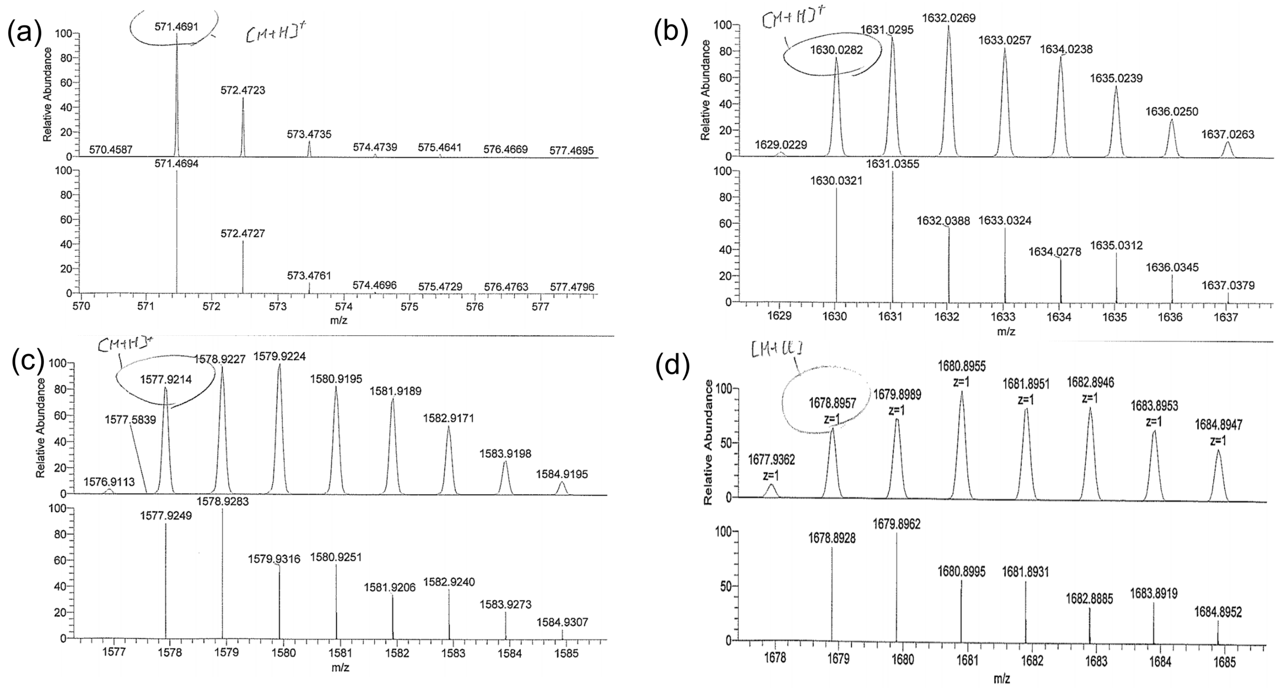

Figure S1. Observed (top) and simulated (bottom) high-resolution MS of (a) **2**, (b) **4**, (c) **5**, and (d) **FL1**.

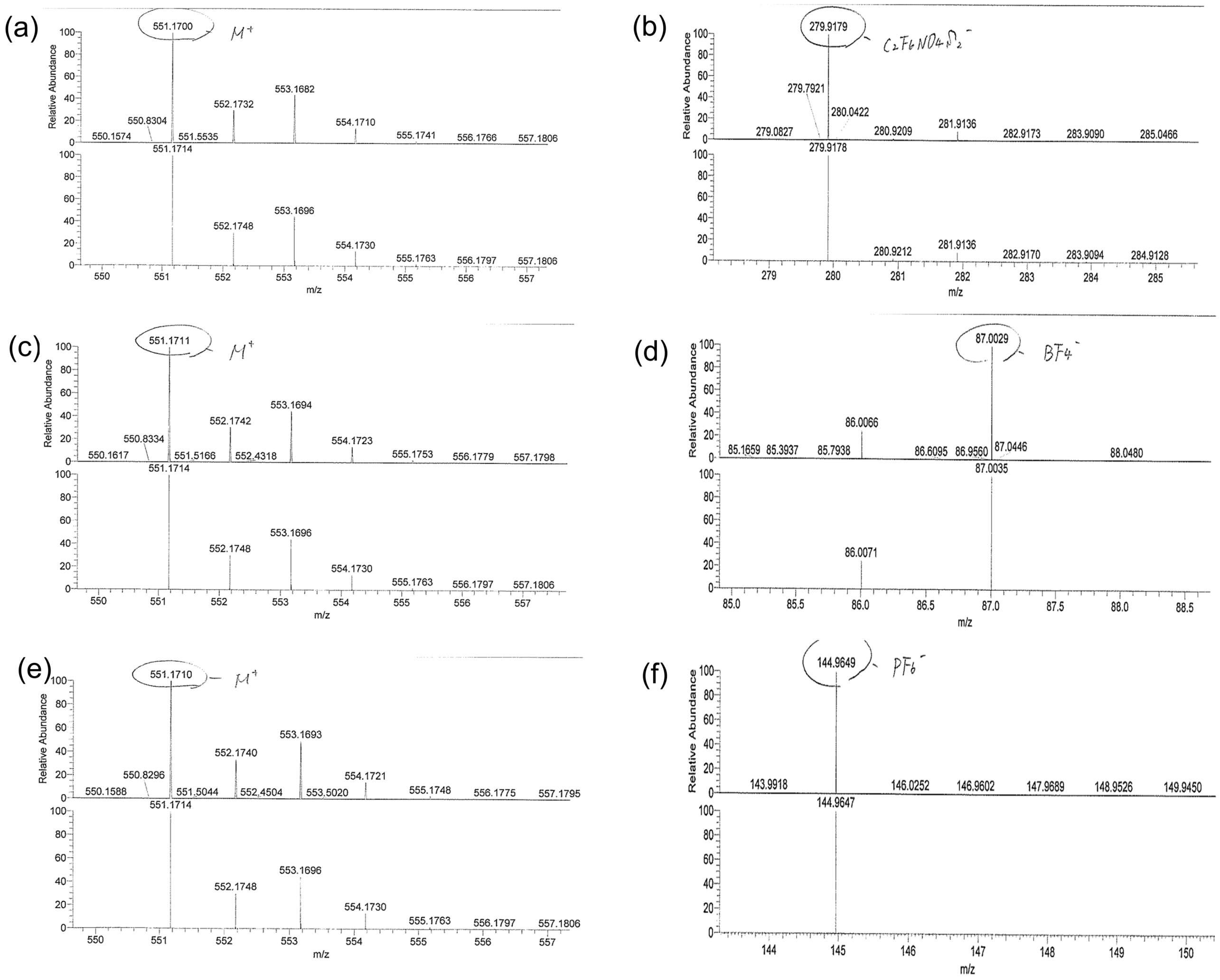

Figure S2. Observed (top) and simulated (bottom) high-resolution MS of (a,b) **[Cu(2MeOby)$_2$][TFSI]**, (c,d) **[Cu(2MeOby)$_2$][BF$_4$]**, and (e,f) **[Cu(2MeOby)$_2$][PF$_6$]**: positive ion mode (a,c,e) and negative ion mode (b,d,f).

4. NMR Spectra

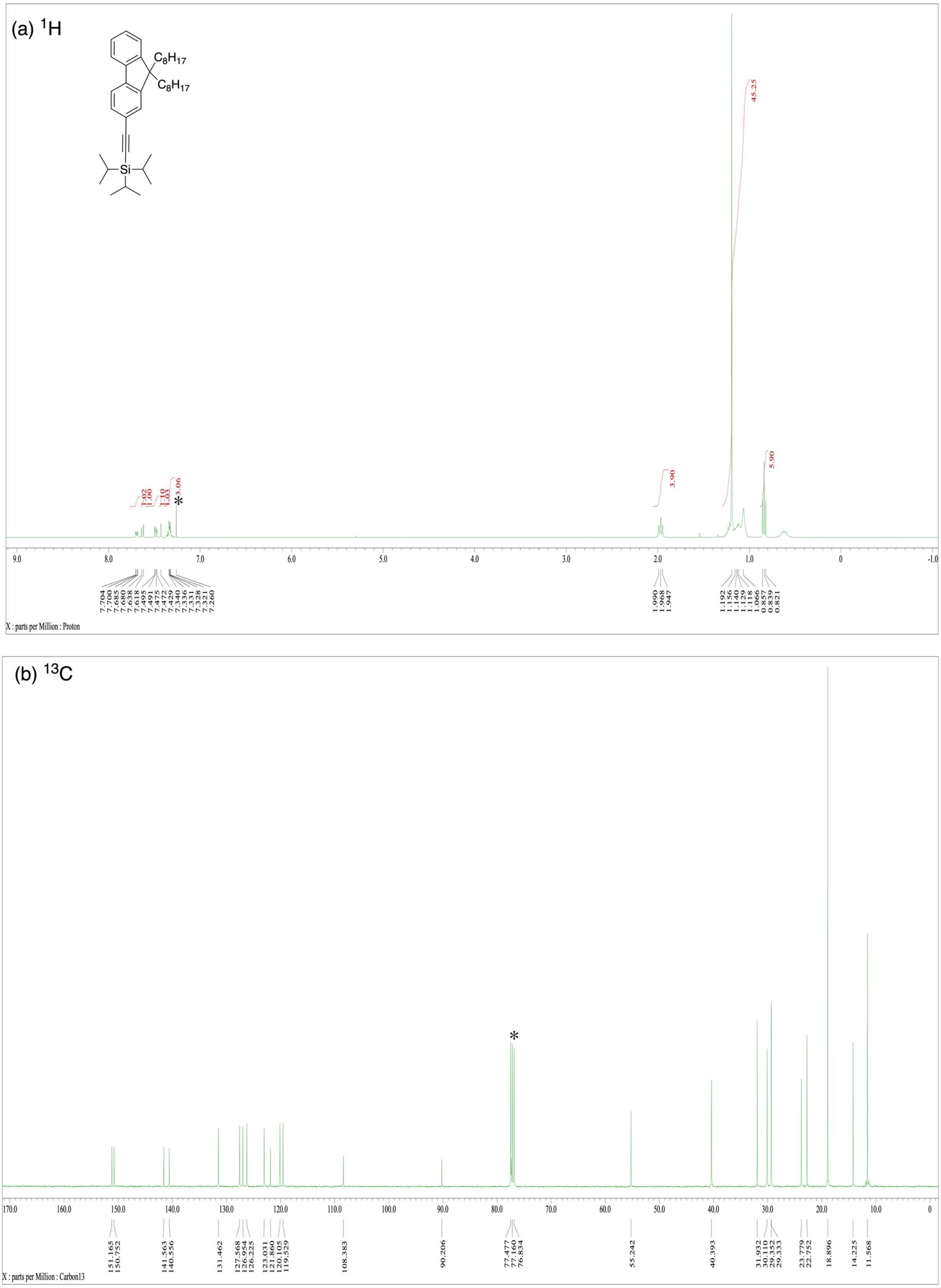

Figure S3. (a) ^{1}H (400 MHz) and (b) ^{13}C (100 MHz) NMR spectra of compound **2** at 25 °C in $CDCl_3$. Peaks marked with ∗ arise from residual solvents.

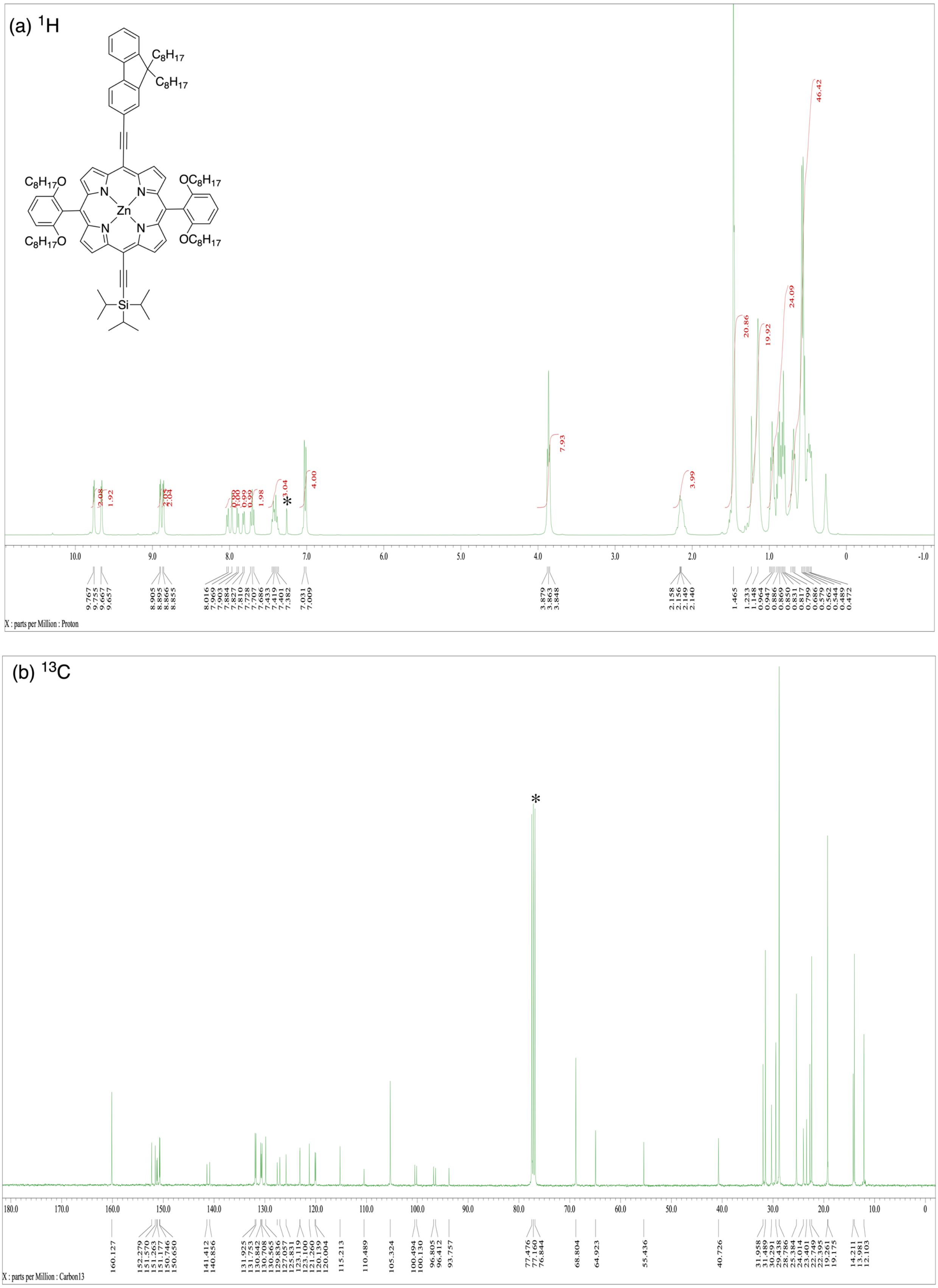

Figure S4. (a) ^{1}H (400 MHz) and (b) ^{13}C (100 MHz) NMR spectra of porphyrin **4** at 25 °C in $CDCl_3$. Peaks marked with ∗ arise from residual solvents.

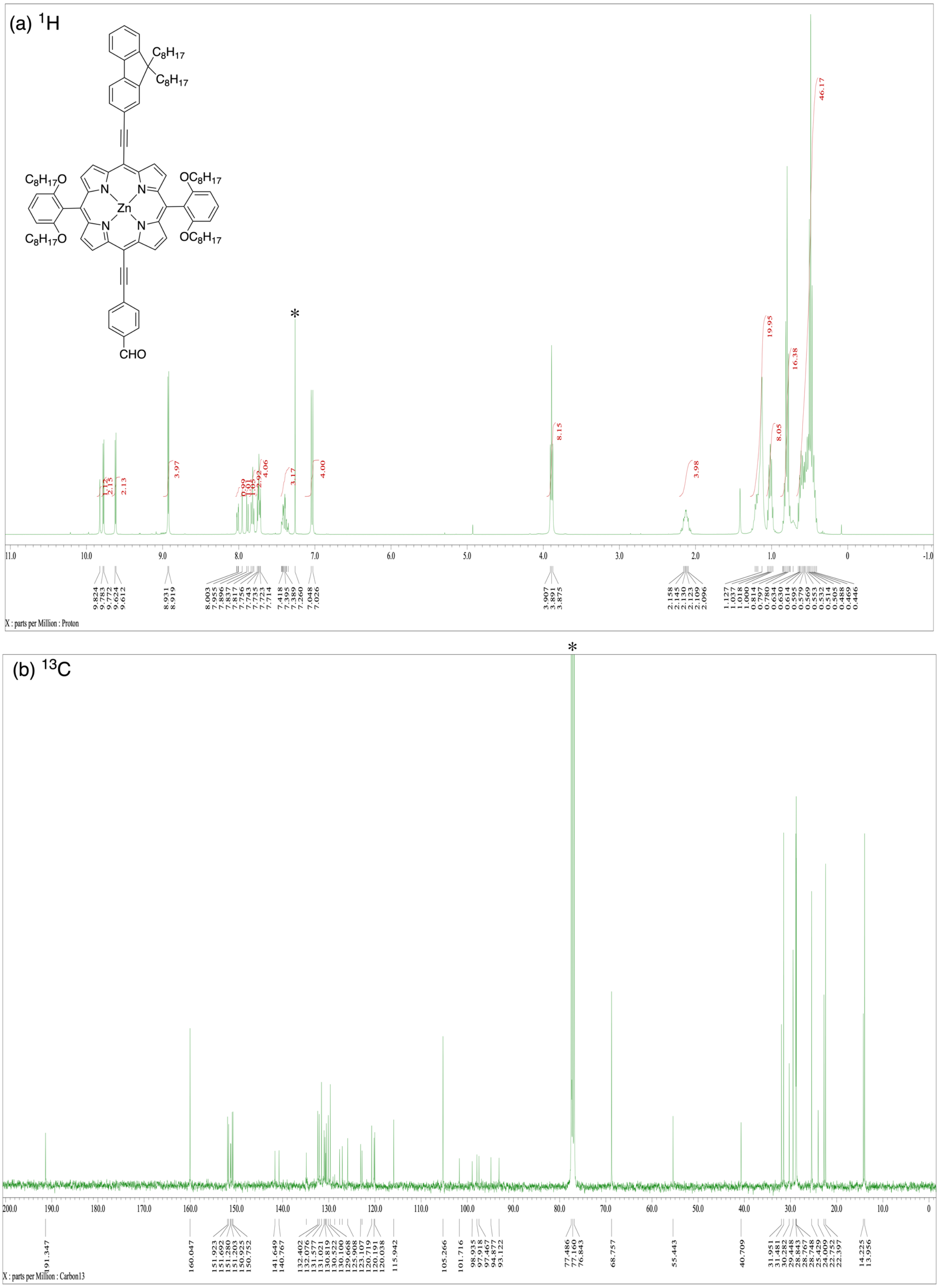

Figure S5. (a) ^{1}H (400 MHz) and (b) ^{13}C (100 MHz) NMR spectra of porphyrin **5** at 25 °C in $CDCl_3$. Peaks marked with $*$ arise from residual solvents.

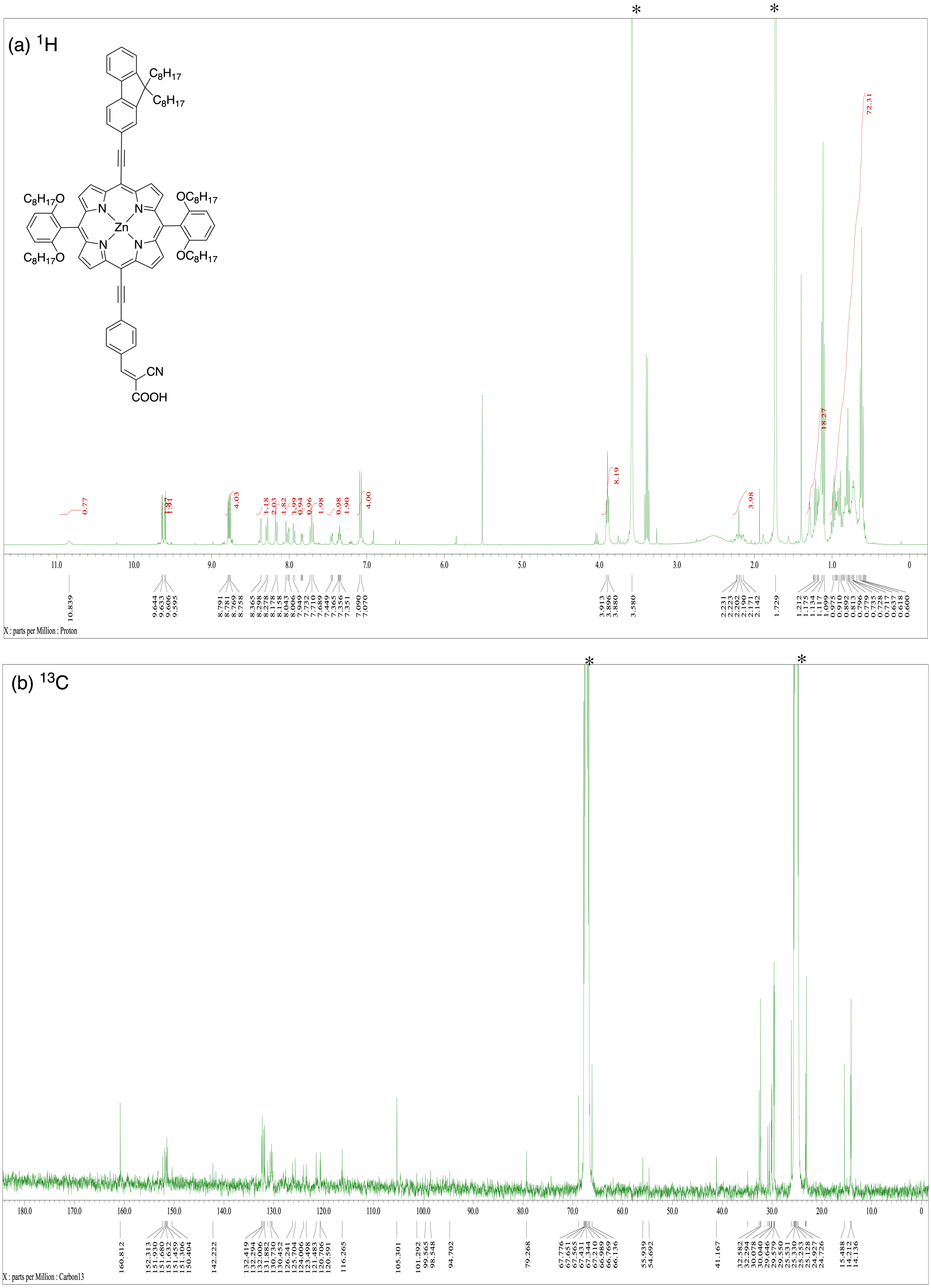

Figure S6. (a) ^{1}H (400 MHz) and (b) ^{13}C (100 MHz) NMR spectra of porphyrin **FL1** at 25 °C in THF-d_8. Peaks marked with $*$ arise from residual solvents.

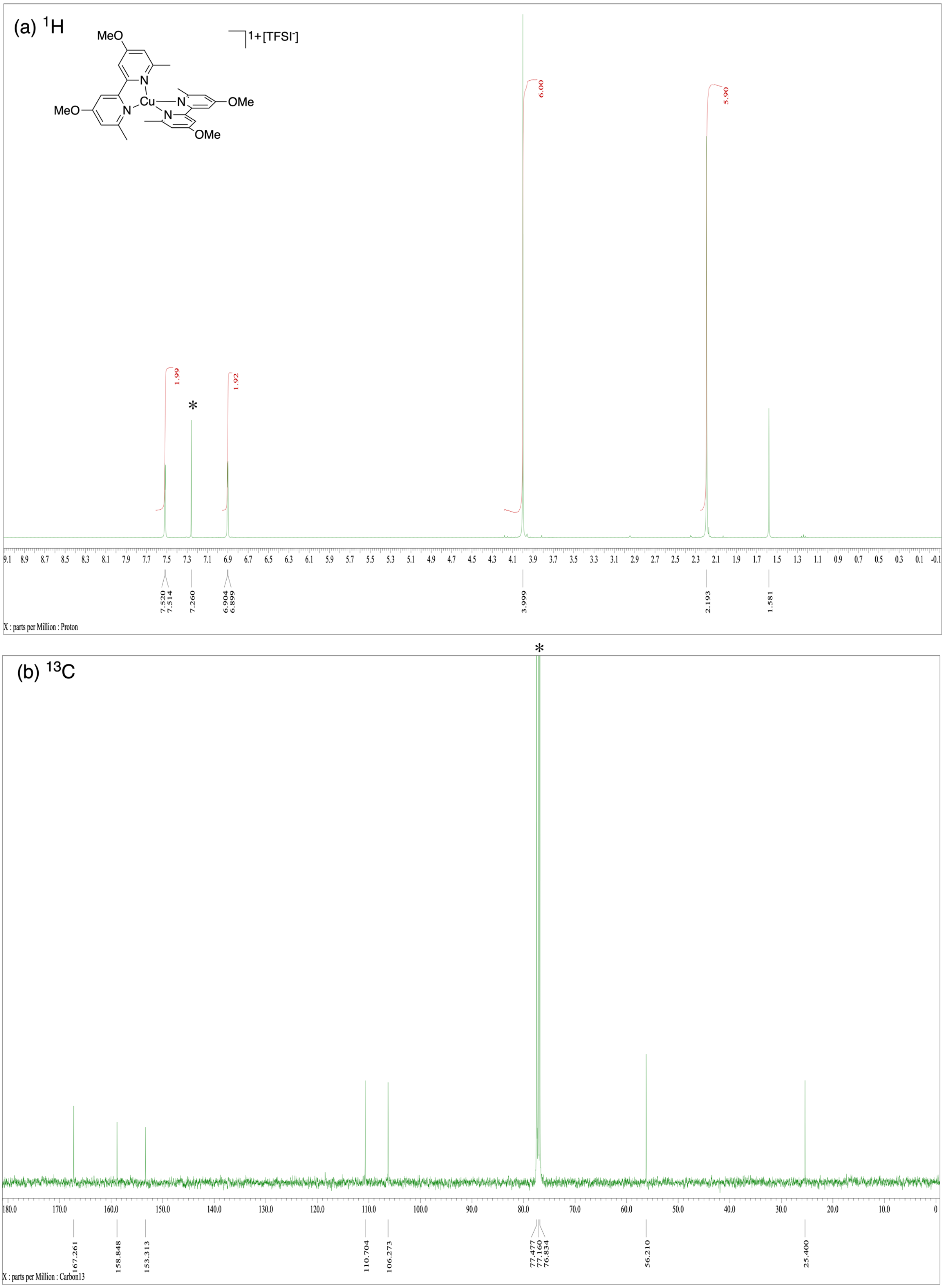

Figure S7. (a) ^{1}H (400 MHz) and (b) ^{13}C (100 MHz) NMR spectra of compound **[Cu(2MeOby)$_2$][TFSI]** at 25 °C in $CDCl_3$. Peaks marked with ∗ arise from residual solvents.

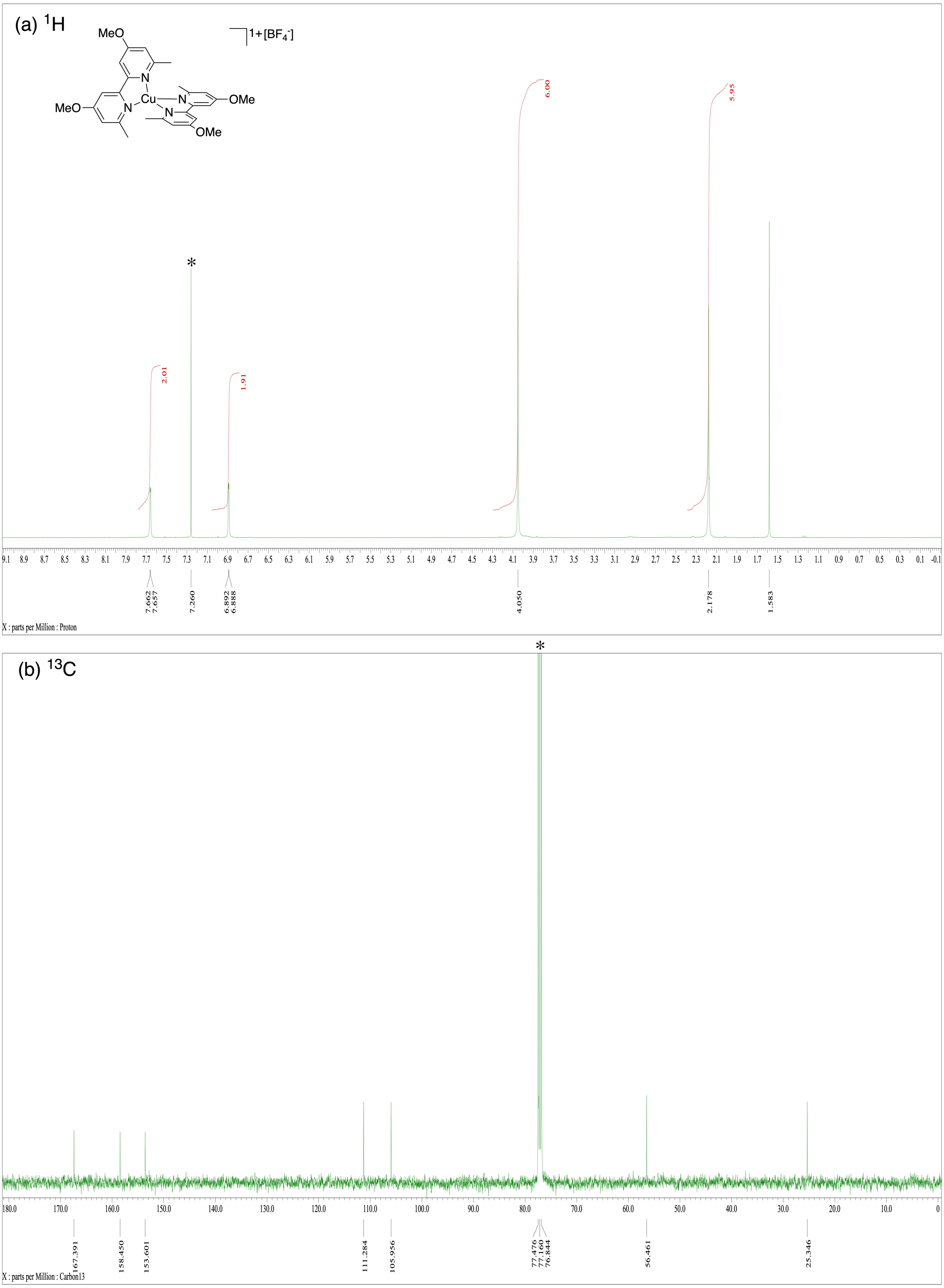

Figure S8. (a) ^{1}H (400 MHz) and (b) ^{13}C (100 MHz) NMR spectra of compound **[Cu(2MeOby)$_2$][BF$_4$]** at 25 °C in CDCl$_3$. Peaks marked with $*$ arise from residual solvents.

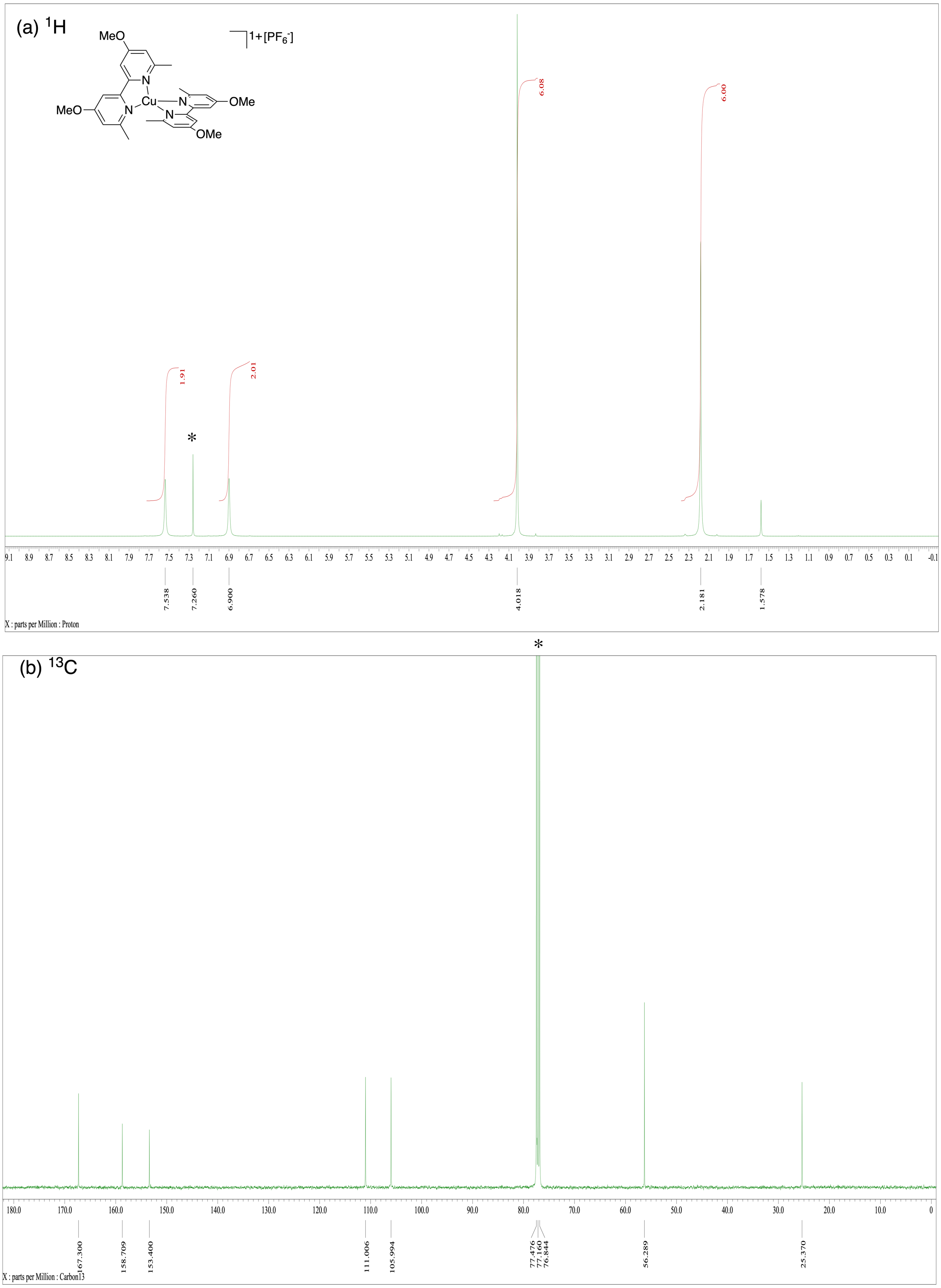

Figure S9. (a) ^{1}H (400 MHz) and (b) ^{13}C (100 MHz) NMR spectra of compound **[Cu(2MeOby)$_2$][PF$_6$]** at 25 °C in CDCl$_3$. Peaks marked with ∗ arise from residual solvents.

5. X-Ray Crystallographic Details

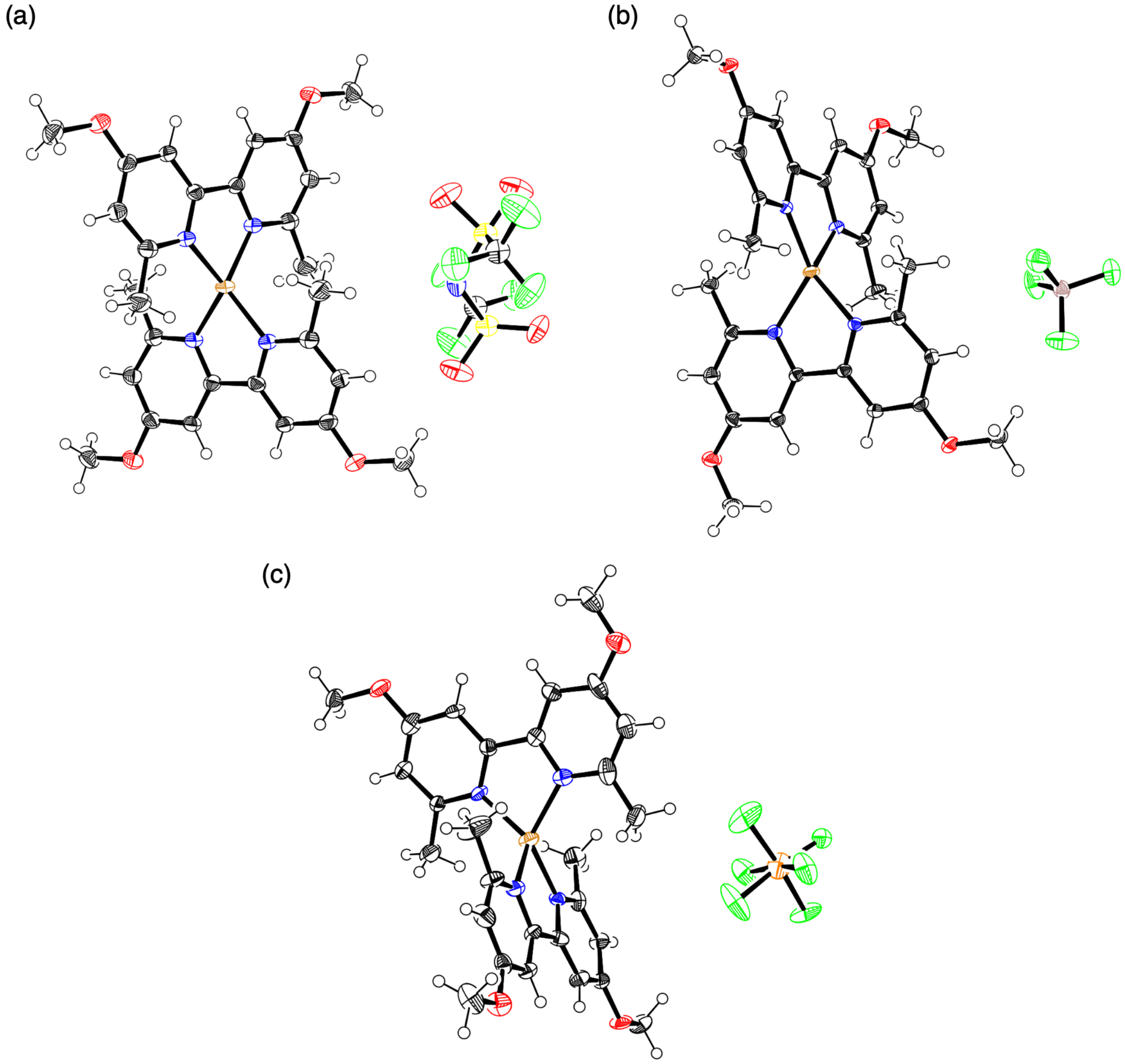

Figure S10. X-Ray crystal structure of (a) **[Cu(2MeOby)$_2$][TFSI]**, (b) **[Cu(2MeOby)$_2$][BF$_4$]**, and (c) **[Cu(2MeOby)$_2$][PF$_6$]**. Thermal ellipsoids represent 50% probability. Minor disorder components of the counterions are omitted for clarity.

Table S1. Crystal data of copper(I) complexes.

	[Cu(2MeOby)$_2$][TFSI]	**[Cu(2MeOby)$_2$][BF$_4$]**	**[Cu(2MeOby)$_2$][PF$_6$]**
formula	0.25($C_{28}H_{32}CuN_4O_4$)· 0.25($C_2F_6NO_4S_2$)	$C_{28}H_{32}CuN_4O_4 \cdot BF_4$	$C_{28}H_{32}CuN_4O_4 \cdot F_6P$
M_r	208.07	638.92	697.08
T [K]	143(2)	143(2)	143(2)
crystal system	orthorhombic	monoclinic	triclinic
space group	*I*bam (No.72)	$P2_1/c$ (No.14)	*P*-1 (No.2)
a [Å]	8.071(2)	14.6532(4)	9.7349(8)
b [Å]	16.120(4)	11.4428(3)	11.1899(10)
c [Å]	26.964(8)	16.8771(5)	15.3441(12)
α [°]	90	90	73.793(8)
β [°]	90	95.086(3)	74.976(7)
γ [°]	90	90	88.820(7)
V [Å^3]	3508.1(16)	2818.70(14)	1547.8(2)
Z	16	4	2
ρ_{calcd} [g cm^{-3}]	1.576	1.506	1.496
F [000]	1704	1320	716
crystal size [mm^3]	0.30×0.20×0.10	0.30×0.20×0.10	0.28×0.03×0.01
$2\theta_{\mathrm{max}}$ [°]	54.95	55.00	52.00
reflections collected	13214	21905	11574
independent	2055	6479	5949
parameters	150	387	469
R_1 [$I > 2\sigma(I)$]	0.0556	0.0453	0.1232
wR_2 [all data]	0.2108	0.1104	0.3925
GOF	1.056	1.065	1.086
CCDC number	2451025	2451027	2451026

6. Optical and Electrochemical Properties of Porphyrin Dyes

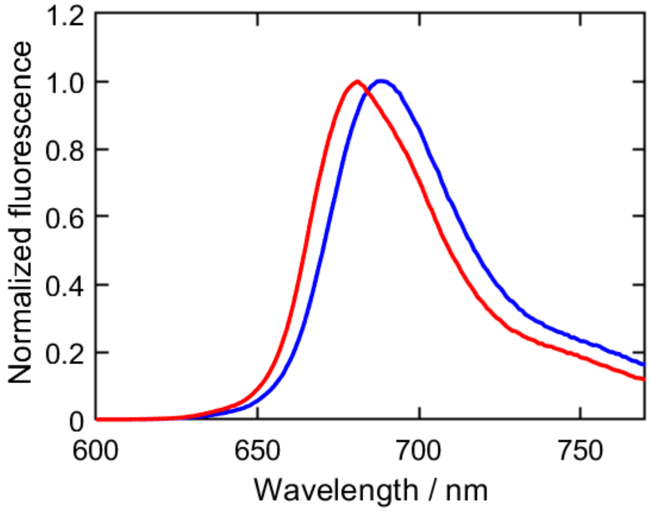

Figure S11. Fluorescence spectra of **FL1**(red), and **LG4**[S12] (blue) in THF. The samples were excited at wavelengths for Soret band maxima.

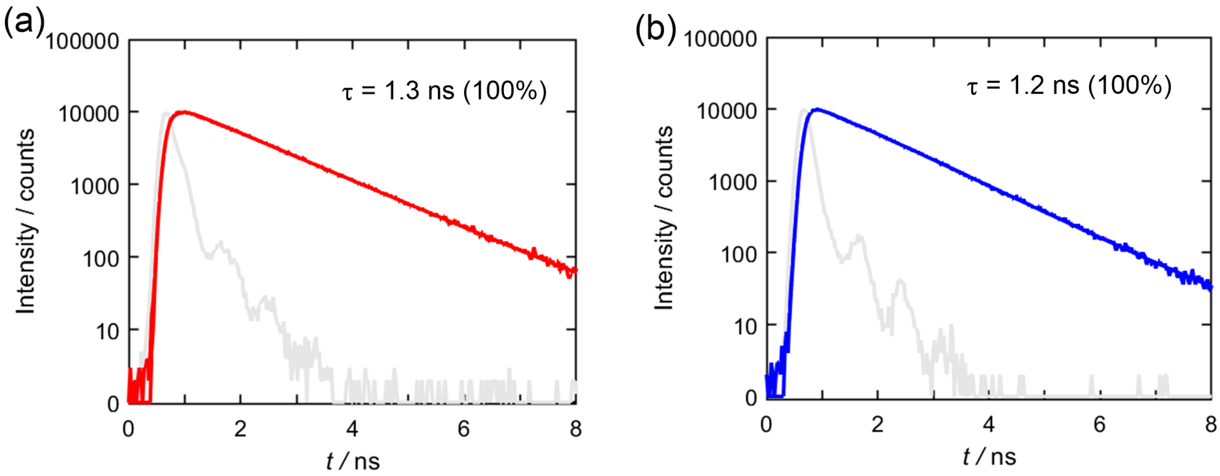

Figure S12. Fluorescence decays of spectra of (a) **FL1** (red), and (b) **LG4** (red) in THF. The samples were excited at 416 nm. The monitoring wavelengths are 681 nm, and 688 nm, respectively. The solid lines present decay fittings and the gray lines show the instrumental response function. The fluorescence lifetimes (τ) are given in the figures.

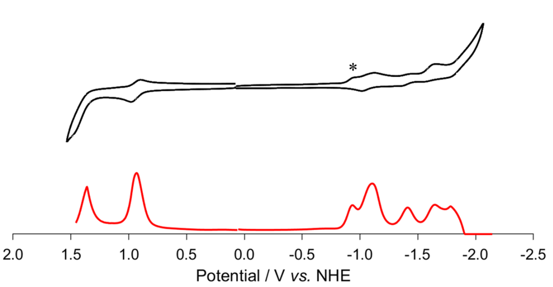

Figure S13. Cyclic voltammograms (black) and differential pulse voltammetry (DPV) curves (red) of porphyrins (a) **FL1**, and (b) **LG4**. Redox potentials were determined by DPV. Solvent: THF; scan rate: 0.1 V s^{-1}; working electrode: glassy carbon; reference electrode: Ag/Ag^+ (sat. KCl); electrolyte: 0.1 M *n*-Bu_4NPF_6. Peaks marked with ∗ arise from oxygen

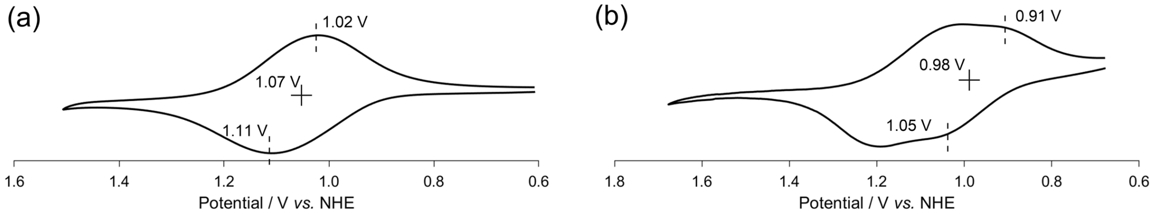

Figure S14. Cyclic voltammograms curves of porphyrins (a) **FL1**, and (b) **LG4** absorbed on TiO_2 film. Solvent: Acetonitrile; scan rate: 0.1 V s^{-1}; working electrode: glassy carbon; reference electrode: Ag/Ag^+ (sat. KCl); electrolyte: 0.1 M LiTFSI.

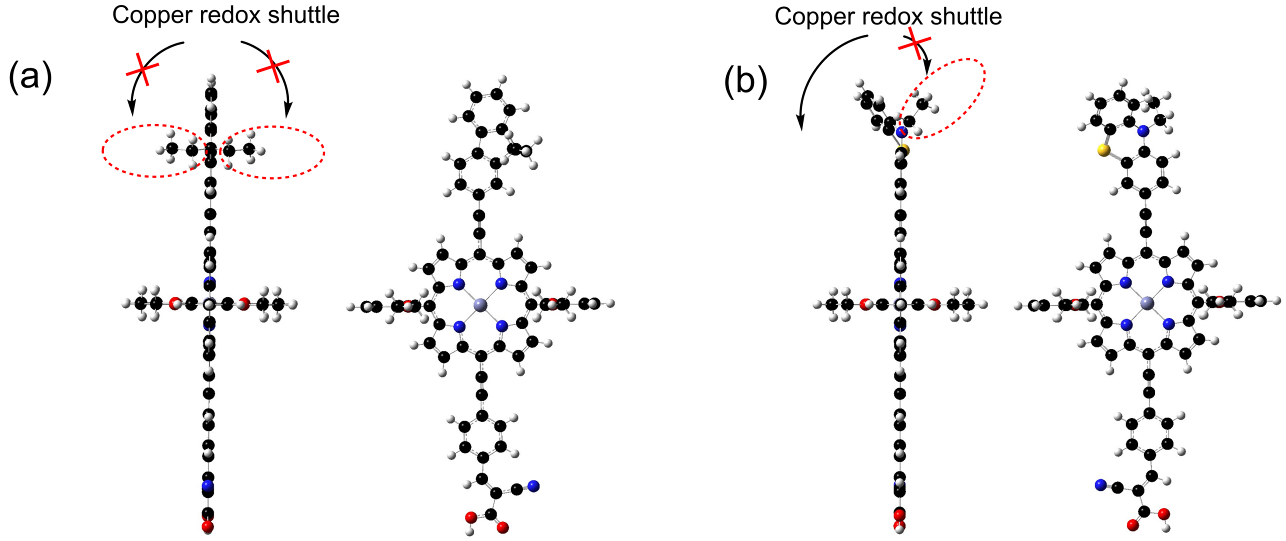

Figure S15. The optimized structures for (a) **FL1**, and (b) **LG4**. To simplify the calculations, octyl groups on the donor side were replaced with ethyl groups, octyloxy groups on the meso-aryl groups were replaced with the methoxy groups.

7. Optical and Electrochemical Properties of Copper Complexes

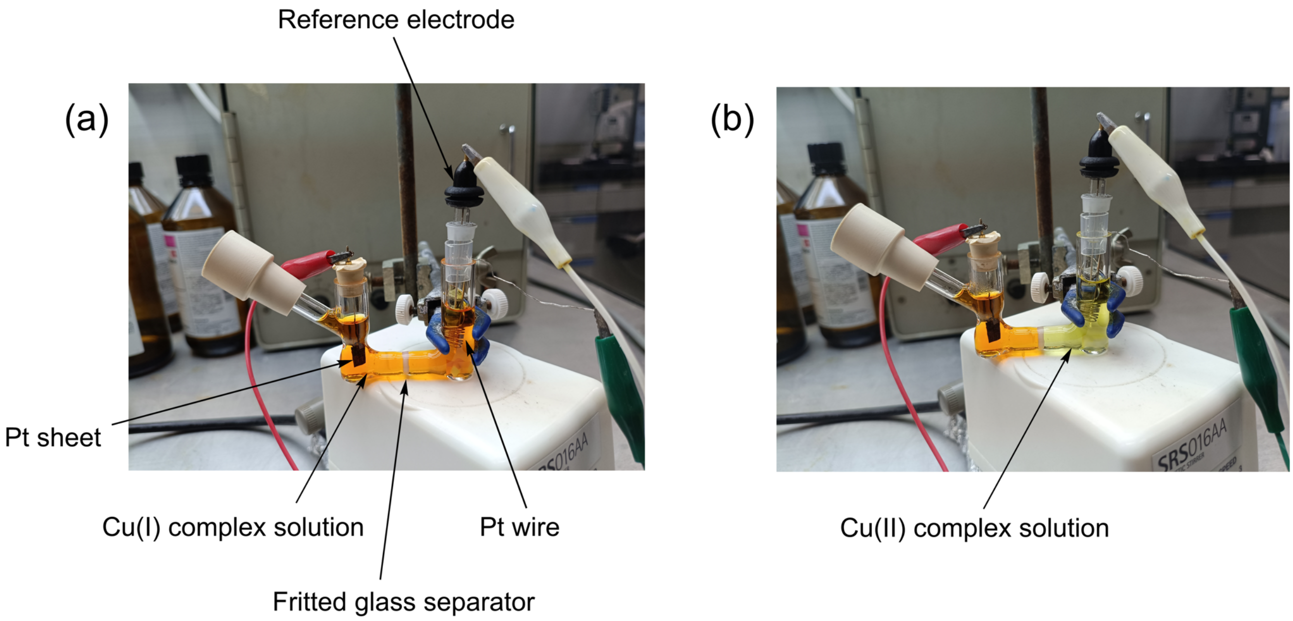

Figure S16. The experimental setup for the bulk electrosynthesis of copper(II) complexes: (a) the initial state and (b) the final state. The copper(I) complex **[Cu(2MeOby)$_2$][BF$_4$]** was used as the starting material in these pictures. The pale-yellow solution in the right compartment after the electrolysis is the pure **[Cu(2MeOby)$_2$][BF$_4$]$_2$** solution in acetonitrile**.**

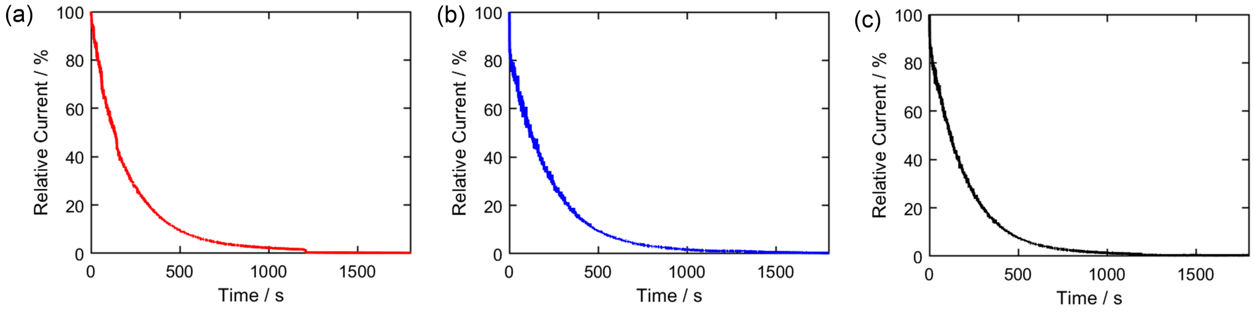

Figure S17. Plot of the relative current *vs*. time for the bulk electrolysis of (a) **[Cu(2MeOby)$_2$][TFSI]**, (b) **[Cu(2MeOby)$_2$][BF$_4$]**, and (c) **[Cu(2MeOby)$_2$][PF$_6$]**.

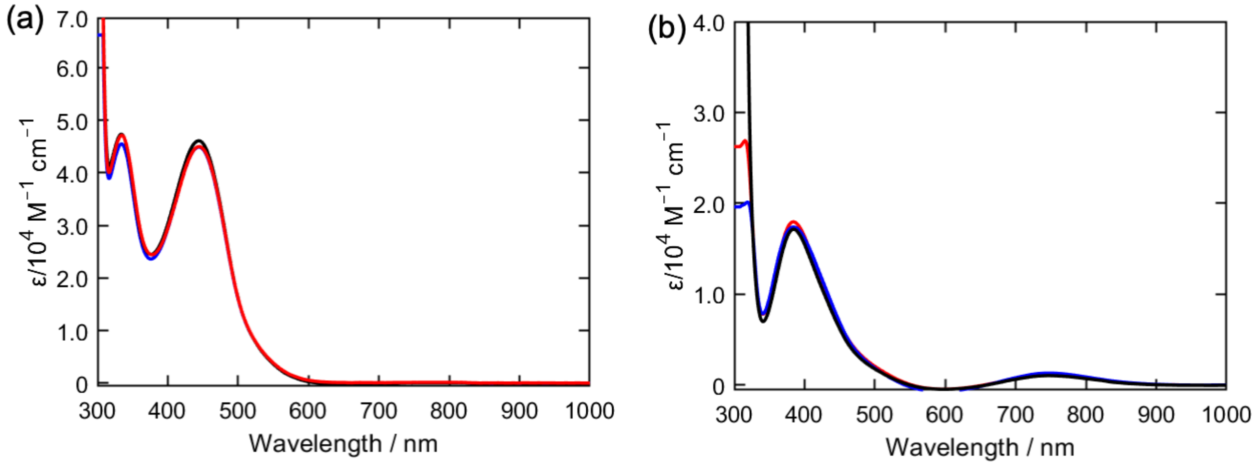

Figure S18. UV/vis/NIR absorption spectra of (a) **[Cu(2MeOby)$_2$][X]** (X = TFSI (red), BF$_4$ (blue), and PF$_6$ (black)), and (b) **[Cu(2MeOby)$_2$][X]$_2$** in the presence of 0.1 M LiX (X = TFSI (red), BF$_4$ (blue), and PF$_6$ (black)) in acetonitrile.

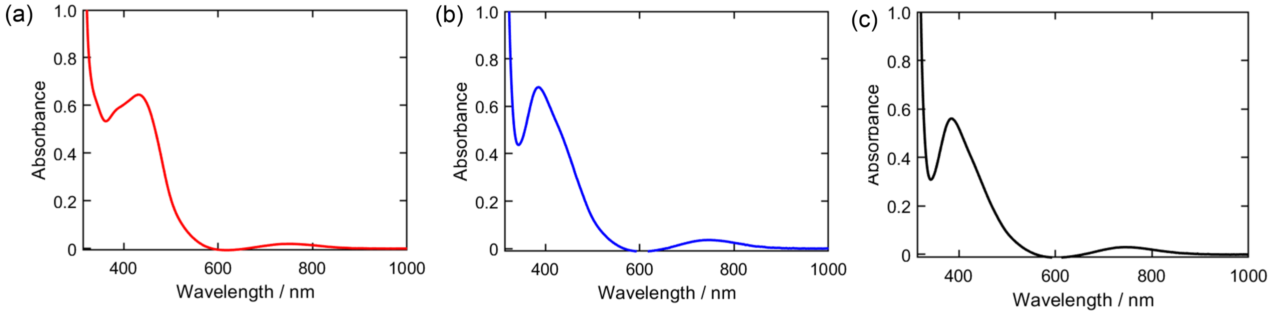

Figure S19. UV/vis/NIR absorption spectra of the as-prepared copper(II) complexes: (a) **[Cu(2MeOby)$_2$][TFSI]$_{1.6}$** (1.86 mg as-prepared samples in 6.5 mL acetonitrile), (b) **[Cu(2MeOby)$_2$][BF$_4$]$_{1.9}$** (1.29 mg as-prepared samples in 5.0 mL acetonitrile**)**, and (c) **[Cu(2MeOby)$_2$][PF$_6$]$_{1.9}$** (1.72 mg as-prepared samples in 6.5 mL acetonitrile).

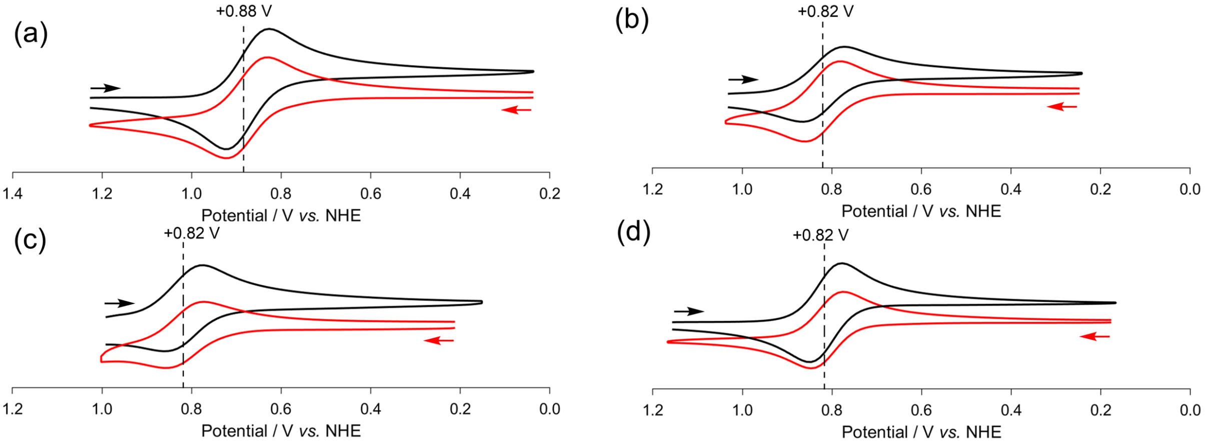

Figure S20. Cyclic voltammograms of (a) **[Cu(tmby)$_2$][TFSI]/[Cu(tmby)$_2$][TFSI]$_2$**, (b) **[Cu(2MeOby)$_2$][TFSI]/[Cu(2MeOby)$_2$][TFSI]$_2$**, (c) **[Cu(2MeOby)$_2$][BF$_4$]/[Cu(2MeOby)$_2$][BF$_4$]$_2$**, and (d) **[Cu(2MeOby)$_2$][PF$_6$]/[Cu(2MeOby)$_2$][PF$_6$]$_2$**. Red lines represent Cu(I) complex, and black lines represent Cu(II) complex. Solvent: Acetonitrile; scan rate: 0.1 V s^{-1}; working electrode: glassy carbon; reference electrode: Ag/Ag$^+$ (sat. KCl); electrolyte: (a,b) 0.1 M LiTFSI, (c) 0.1 M LiBF$_4$, and (d) 0.1 M LiPF$_6$.

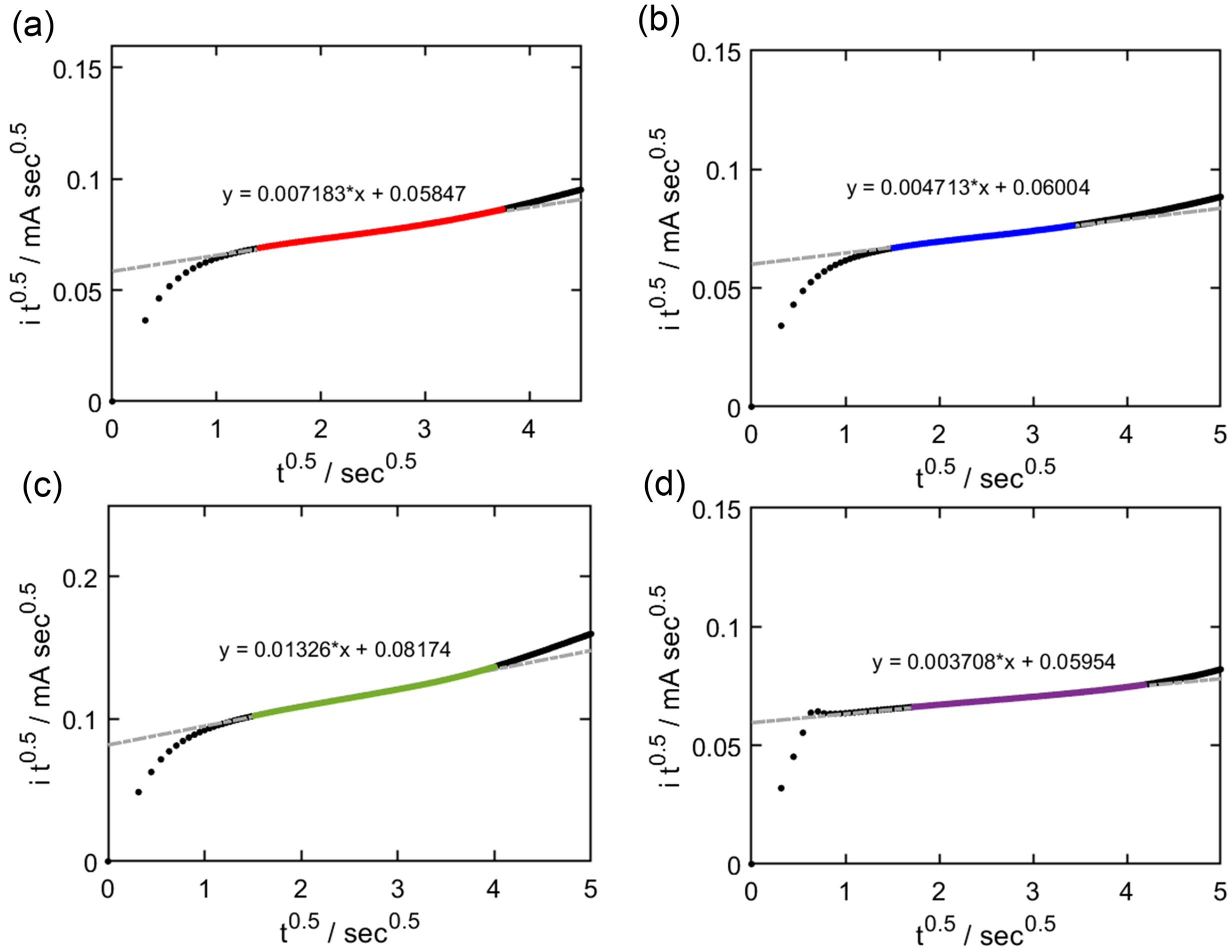

Figure S21. Plot of $it^{0.5}$ *vs.* $t^{0.5}$ for the oxidization of (a) **[Cu(2MeOby)$_2$][TFSI]** containing 0.1 M LiTFSI, (b) **[Cu(2MeOby)$_2$][BF$_4$]** containing 0.1 M LiBF$_4$, (c) **[Cu(2MeOby)$_2$][PF$_6$]** containing 0.1 M LiPF$_6$, and (d) **[Cu(tmby)$_2$][TFSI]** containing 0.1 M LiTFSI in acetonitrile. The concentration of Cu(I) species is 5 mM, and the working area is 0.061 cm^{-2}.

8. Photovoltaic Properties

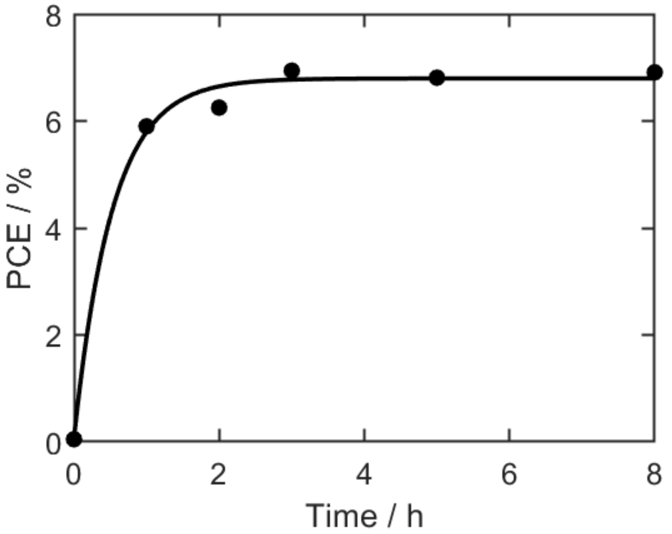

Figure S22. Plots of PCE values as a function of immersion time for DSSCs with **FL1** using **[Cu(tmby)$_2$][TFSI]/[Cu(tmby)$_2$][TFSI]$_2$**. **FL1** dyes were adsorbed on the TiO$_2$ films by immersing them into an EtOH/Toluene (v/v = 5/1) solution of **FL1** dyes at 25 °C without co-adsorbent.

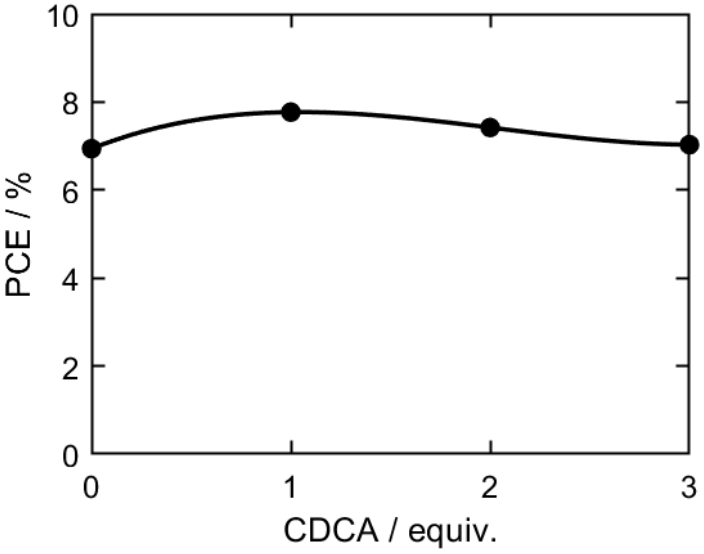

Figure S23. Plots of the PCE values as a function of immersion time for DSSCs with **FL1** **[Cu(tmby)$_2$][TFSI]/[Cu(tmby)$_2$][TFSI]$_2$**. **FL1** dyes were adsorbed on the TiO$_2$ films by immersing them into an EtOH/Toluene (v/v = 5/1) solution of **FL1** dyes for 3 h at 25 °C.

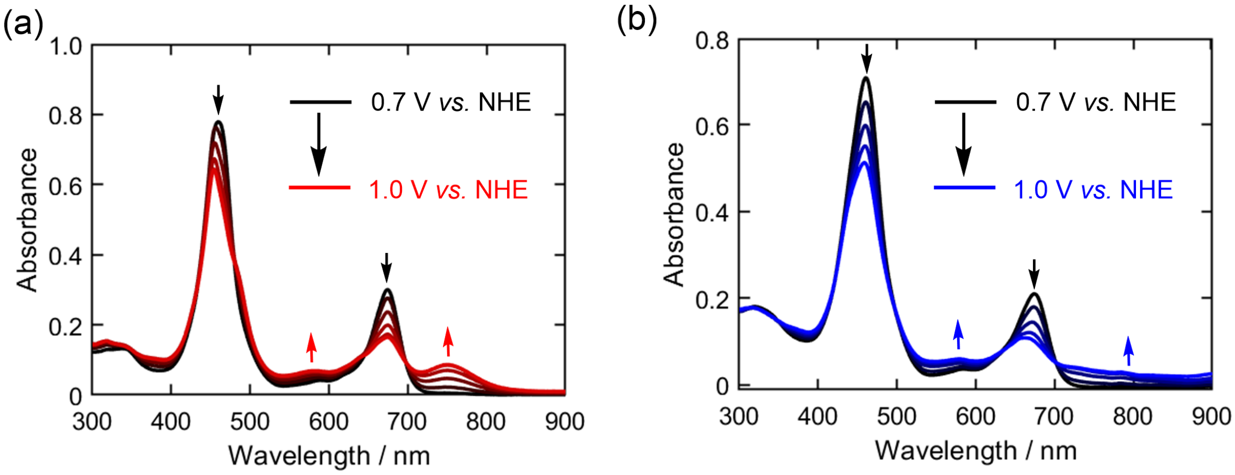

Figure S24. Absorption spectral changes upon electrochemical oxidation of (a) **FL1**, and (b) **LG4** in THF containing 0.1 M *n*-Bu$_4$NPF$_6$. The applied voltages (*vs.* NHE) are also shown.

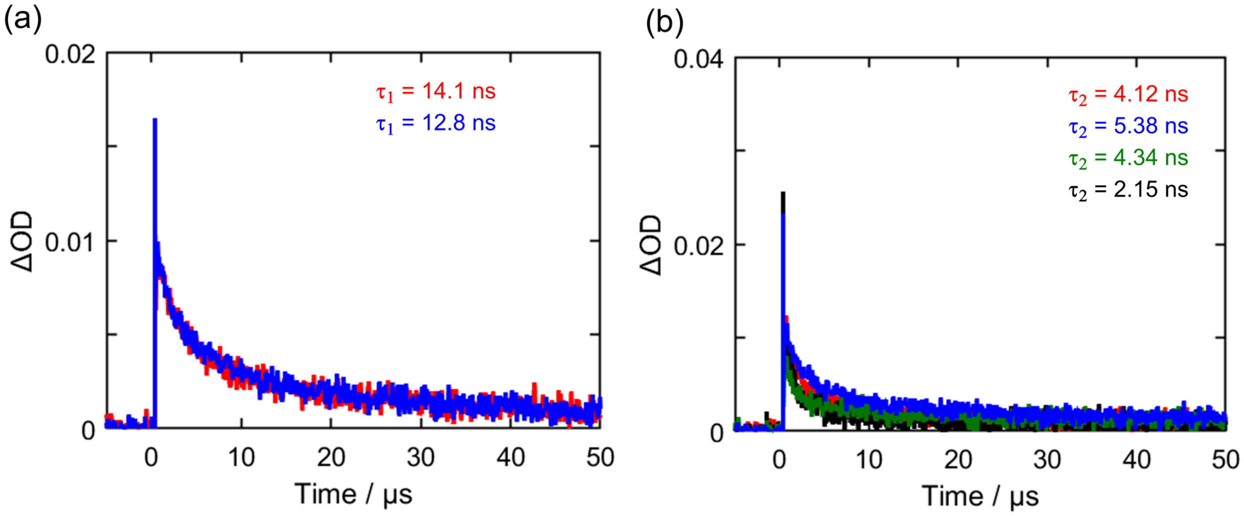

Figure S25. Time-resolved transient absorption profiles of the TiO$_2$ films sensitized with **FL1** (red), and **LG4** (blue) with (a) neat acetonitrile (0.1 M LiTFSI, 0.5 M TBP) and (b) **[Cu(tmby)$_2$][TFSI]/[Cu(tmby)$_2$][TFSI]$_2$** (red for **FL1** and blue for **LG4**) or **[Cu(2MeOby)$_2$][TFSI]/[Cu(2MeOby)$_2$][TFSI]$_2$** (black for **FL1** and green for **LG4**) redox shuttle (0.2 M **[CuL$_2$][TFSI]**, 0.05 M **[CuL$_2$][TFSI]$_2$**, 0.1 M LiTFSI, and 0.5 M TBP (L = **tmby** or **2MeOby**)). The samples were excited at 540 nm and the decay profiles were monitored at 800 nm.

Table S2. Lifetimes of dye radical cations ($ZnP^{•+}$) and dye regeneration efficiency

dye	τ_1 / μs	τ_2 / μs	ϕ_{reg} / %
LG4[a]	12.8	5.38	58
LG4[b]	12.8	4.34	66
FL1[a]	14.1	4.12	71
FL1[b]	14.1	2.15	84

[a] τ_2 is determined under **[Cu(tmby)$_2$][TFSI]/[Cu(tmby)$_2$][TFSI]$_2$** redox shuttle. [b] τ_2 is determined under **[Cu(2MeOby)$_2$][TFSI]/[Cu(2MeOby)$_2$][TFSI]$_2$** redox shuttle.

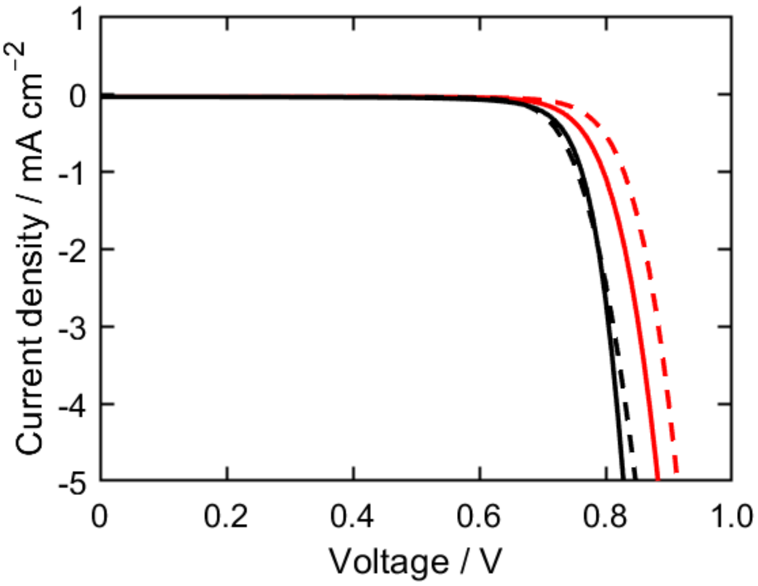

Figure S26. Current-voltage characteristics of the DSSCs with **FL1** (red dashed line), and **LG4** (black dashed line) using **[Cu(tmby)$_2$][TFSI]/[Cu(tmby)$_2$][TFSI]$_2$** redox shuttle, and with **FL1** (red solid line), and **LG4** (black solid line) using **[Cu(2MeOby)$_2$][TFSI]/[Cu(2MeOby)$_2$][TFSI]$_2$** redox shuttle under dark conditions. The composition of the electrolyte solution: 0.2 M **[CuL$_2$][TFSI]**, 0.05 M **[CuL$_2$][TFSI]$_2$**, 0.1 M LiTFSI, and 0.5 M TBP in acetonitrile. (**L** = **tmby** or **2MeOby**)

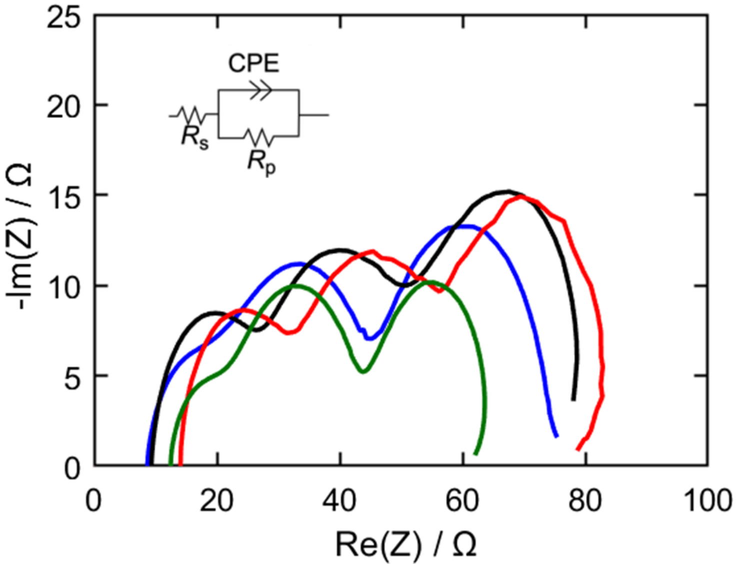

Figure S27. EIS Nyquist Plots of DSSCs with **FL1** (red), and **LG4** (blue) using **[Cu(tmby)$_2$][TFSI]/[Cu(tmby)$_2$][TFSI]$_2$** redox shuttle, and with **FL1** (black), and **LG4** (green) using **[Cu(2MeOby)$_2$][TFSI]/[Cu(2MeOby)$_2$][TFSI]$_2$** under AM 1.5G illumination at open-circuit conditions The composition of the electrolyte solution: 0.2 M **[CuL$_2$][TFSI]**, 0.05 M **[CuL$_2$][TFSI]$_2$**, 0.1 M LiTFSI, and 0.5 M TBP in acetonitrile (**L** = **tmby** or **2MeOby**). The inset is an equivalent Randles circuit impedance model. R_S is the series resistance accounting for transport resistance of transparent conducting oxide (TCO); R_P is the electron transfer resistance for CR at the FTO/TiO$_2$/electrolyte interfaces; while CPE is the constant phase element representing capacitance at the TiO$_2$/electrolyte/interface. The electron transfer resistances (R_P) at the TiO$_2$/dye/electrolyte interface were determined as 45.0 Ω (**FL1** with **[Cu(tmby)$_2$][TFSI]/[Cu(tmby)$_2$][TFSI]$_2$**), 42.5 Ω (**FL1** with **[Cu(2MeOby)$_2$][TFSI]/[Cu(2MeOby)$_2$][TFSI]$_2$**), 36.8 Ω (**LG4** with **[Cu(tmby)$_2$][TFSI]/[Cu(tmby)$_2$][TFSI]$_2$**), and 32.2 Ω (**LG4** with **[Cu(2MeOby)$_2$][TFSI]/[Cu(2MeOby)$_2$][TFSI]$_2$**).

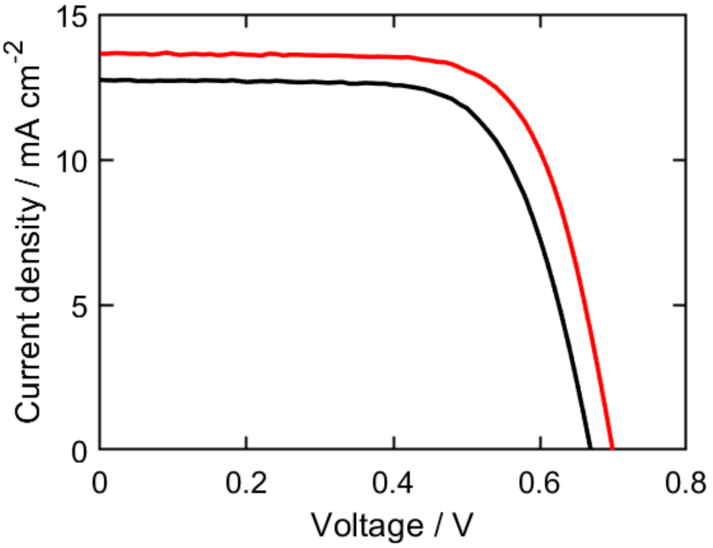

Figure S28. Photocurrent-voltage characteristics of the DSSCs with **FL1** (red) and **LG4** (black) using the I$^-$/I$_3$$^-$ redox shuttle for achieving the highest PCEs. The composition of the electrolyte solution: 0.6 M dimethylpropyl-imidazolium iodide, 0.05 M I$_2$, 0.1 M LiI, and 0.5 M TBP in acetonitrile.

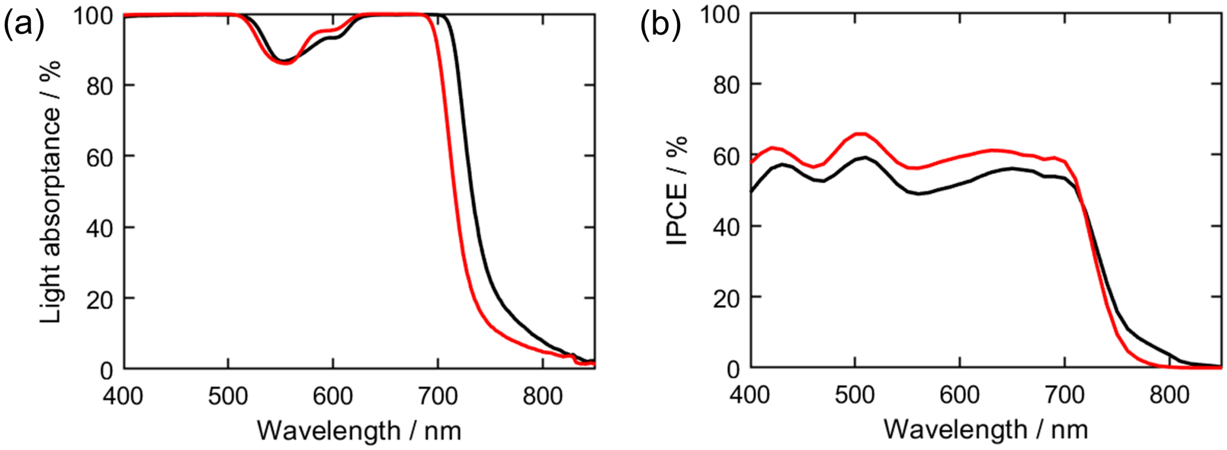

Figure S29. (a) Absorption spectra of the porphyrin-adsorbed TiO$_2$ film (8 μm) of **FL1** (red) and **LG4** (black), and (b) photocurrent action spectra of the DSSCs with **FL1** (red) and **LG4** (black) using the I$^-$/I$_3$$^-$ redox shuttle. The light-scattering TiO$_2$ layers were not used to obtain an accurate absorption profile for the light-harvesting efficiency.

***Table S3*. Photovoltaic performances of the DSSCs under AM1.5 illumination**[a]

dye	J_{SC} / mA cm^{-2}	V_{OC} / V	*ff*	PCE / %
LG4	12.7 (12.5 ± 0.3)	0.670 (0.667 ± 0.004)	0.690 (0.686 ± 0.006)	5.89 (5.73 ± 0.2)
FL1	13.6 (13.5 ± 0.2)	0.700 (0.690 ± 0.009)	0.706 (0.718 ± 0.009)	6.74 (6.66 ± 0.1)

[a] Photovoltaic parameters deriving from the highest PCEs. The values in parentheses denote average values from two or three independent experiments. Error bars represent a standard error of the mean.

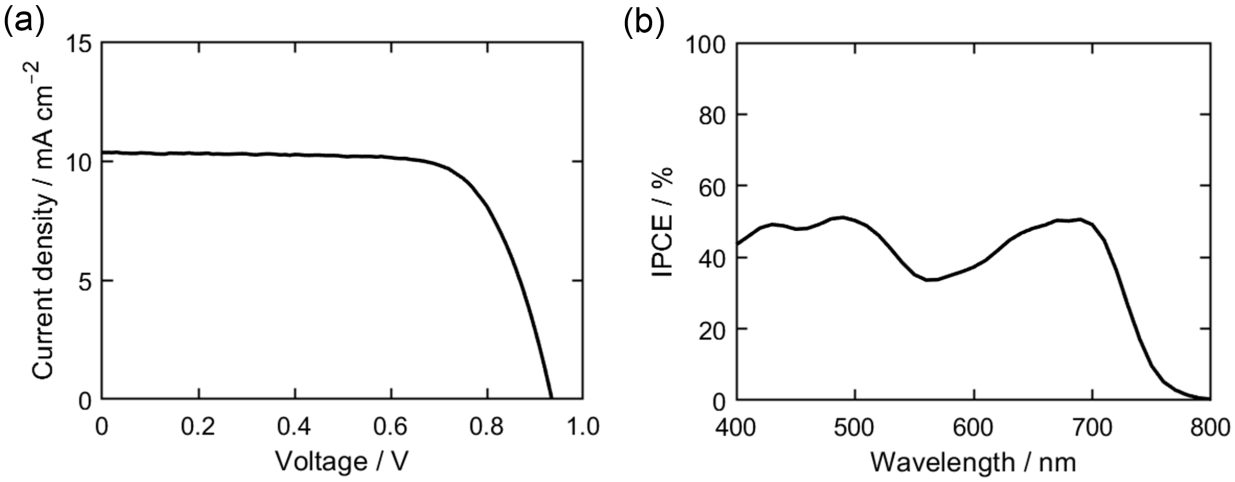

Figure S30. (a) Photocurrent-voltage characteristics and (b) photocurrent action spectrum of the DSSC with **FL1** using **[Cu(tmby)$_2$][TFSI]**/**[Cu(tmby)$_2$][TFSI]$_2$** redox shuttle for achieving the highest PCE. The composition of the electrolyte solution: 0.1 M **[Cu(tmby)$_2$][TFSI]**, 0.025 M **[Cu(tmby)$_2$][TFSI]$_2$**, 0.1 M LiTFSI, and 0.5 M TBP in acetonitrile.

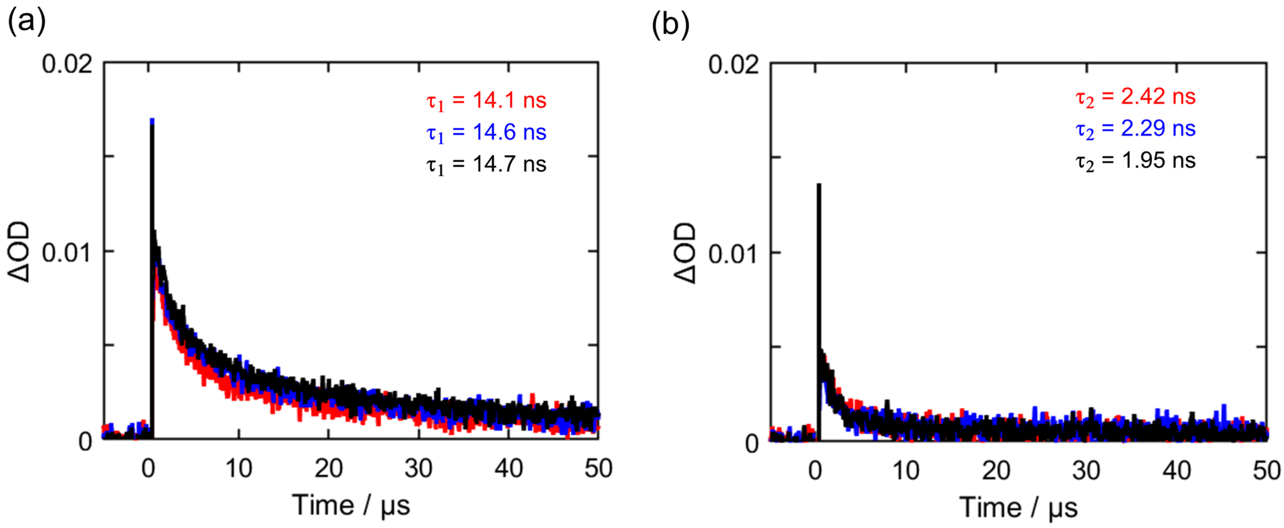

Figure S31. Time-resolved transient absorption profiles of the TiO$_2$ films sensitized based on **FL1** with (a) neat acetonitrile (0.1 M LiX, 0.5 M TBP, X = TFSI (red), BF$_4$ (blue), or PF$_6$ (black)) and (b) **[Cu(2MeOby)$_2$][X]**/**[Cu(2MeOby)$_2$][X]$_2$** redox shuttle (0.1 M **[Cu(2MeOby)$_2$][X]**, 0.025 M **[Cu(2MeOby)$_2$][X]$_2$**, 0.1 M LiX, 0.5 M TBP, X = TFSI (red), BF$_4$ (blue), or PF$_6$ (black)). The samples were excited at 540 nm and the decay profiles were monitored at 800 nm.

Table S4. Lifetimes of dye radical cations ($ZnP^{\bullet+}$) and dye regeneration efficiency

dye	τ_1 / µs	τ_2 / µs	ϕ_{reg} / %
FL1[a]	14.1	2.42	83
FL1[b]	14.6	2.29	84
FL1[c]	14.7	1.95	87

[a] τ_1 is determined under neat acetonitrile (0.1 M LiTFSI and 0.5 M TBP), τ_2 is determined under **[Cu(2MeOby)$_2$][TFSI]/[Cu(2MeOby)$_2$][TFSI]$_2$** redox shuttle (0.1 M **[Cu(2MeOby)$_2$][TFSI]**, 0.025 M **[Cu(2MeOby)$_2$][TFSI]$_2$**, 0.1 M LiTFSI, and 0.5 M TBP).

[b] τ_1 is determined under neat acetonitrile (0.1 M $LiBF_4$ and 0.5 M TBP), τ_2 is determined under **[Cu(2MeOby)$_2$][BF$_4$]/[Cu(2MeOby)$_2$][BF$_4$]$_2$** redox shuttle (0.1 M **[Cu(2MeOby)$_2$][BF$_4$]**, 0.025 M **[Cu(2MeOby)$_2$][BF$_4$]$_2$**, 0.1 M $LiBF_4$, and 0.5 M TBP).

[c] τ_1 is determined under neat acetonitrile (0.1 M $LiPF_6$, and 0.5 M TBP), τ_2 is determined under **[Cu(2MeOby)$_2$][PF$_6$]/[Cu(2MeOby)$_2$][PF$_6$]$_2$** redox shuttle (0.1 M **[Cu(2MeOby)$_2$][PF$_6$]**, 0.025 M **[Cu(2MeOby)$_2$][PF$_6$]$_2$**, 0.1 M $LiPF_6$, and 0.5 M TBP).

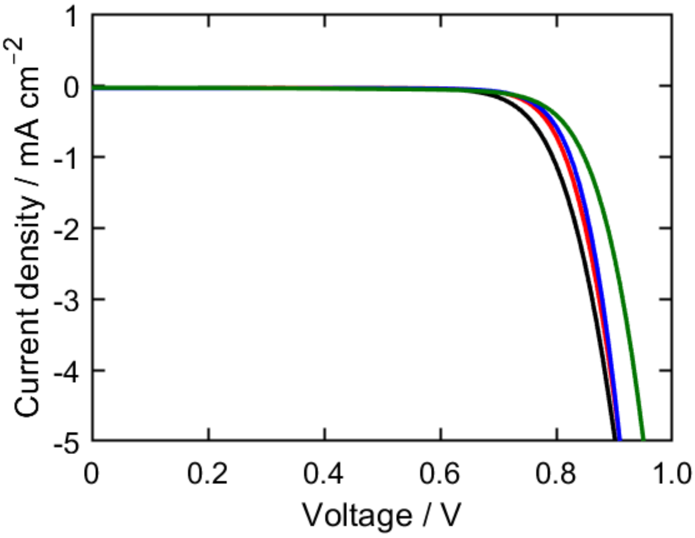

Figure S32. Current-voltage characteristics of the DSSCs with **FL1** using **[Cu(2MeOby)$_2$][X]/[Cu(2MeOby)$_2$][X]$_2$** (X = TFSI (red), BF_4 (blue), or PF_6 (black)), and the DSSC with **FL1+XY1B** using **[Cu(2MeOby)$_2$][PF$_6$]/[Cu(2MeOby)$_2$][PF$_6$]$_2$** (green) under dark conditions. The composition of the electrolyte solution: 0.1 M **[Cu(2MeOby)$_2$][X]**, 0.025 M **[Cu(2MeOby)$_2$][X]$_2$**, 0.1 M LiX, 0.5 M TBP, X = TFSI (red), BF_4 (blue), or PF_6 (black).

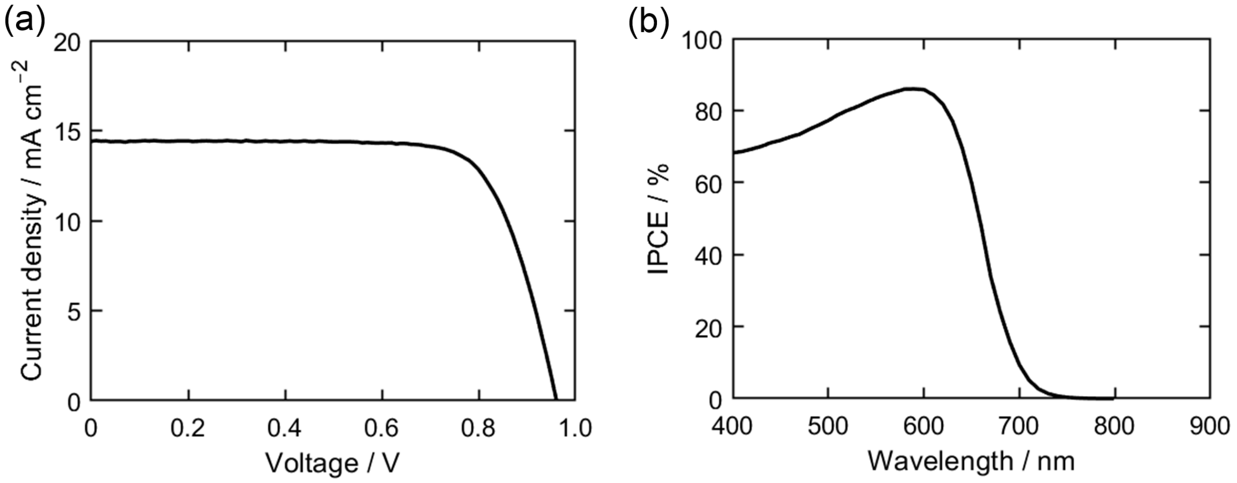

Figure S33. (a) Photocurrent-voltage characteristics and (b) photocurrent action spectrum of the DSSC with **XY1B** for achieving the highest PCE. The redox shuttle is **[Cu(2MeOby)$_2$][PF$_6$]/[Cu(2MeOby)$_2$][PF$_6$]$_2$** (0.1 M **[Cu(2MeOby)$_2$][PF$_6$]**, 0.025 M **[Cu(2MeOby)$_2$][PF$_6$]$_2$**, 0.1 M LiPF$_6$, and 0.5 M TBP). The sensitizer was adsorbed on the TiO$_2$ electrode by immersing the electrode into a THF and ethanol solution (v/v = 1/4) of 0.1 mM **XY1B** at 25 °C for 3 h with 5 mM CDCA coadsorbent.

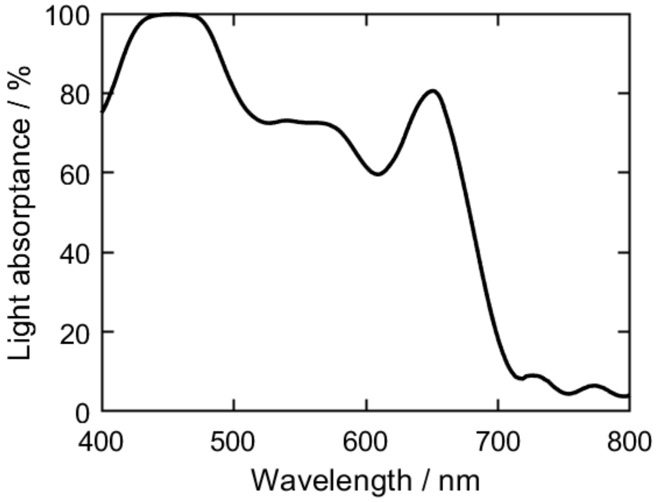

Figure S34. Absorption spectra of the co-sensitized TiO$_2$ film (2 μm) of **FL1+XY1B**. The light-scattering TiO$_2$ layers were not used to obtain an accurate absorption profile for the light-harvesting efficiency.

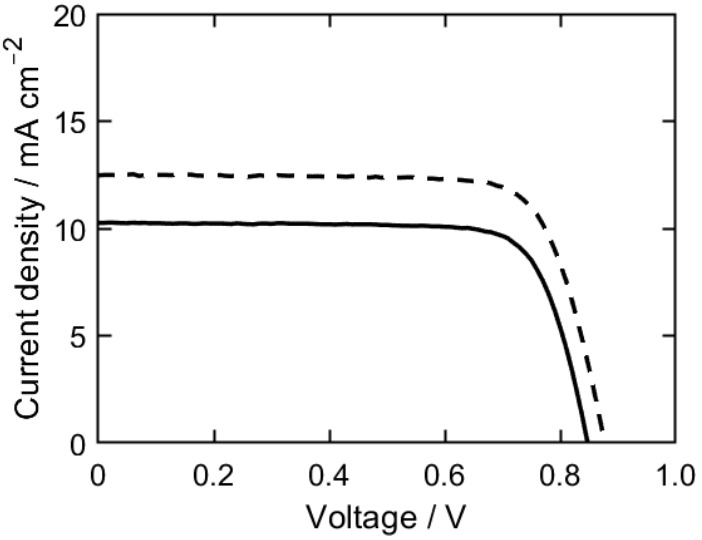

Figure S35. Photocurrent-voltage characteristics of the DSSCs based on **LG4** (black solid line), and **LG4+XY1B** (black dash line) under the best conditions for achieving the highest PCEs with **[Cu(2MeOby)$_2$][PF$_6$]/[Cu(2MeOby)$_2$][PF$_6$]$_2$** redox shuttle (0.1 M **[Cu(2MeOby)$_2$][PF$_6$]**, 0.025 M **[Cu(2MeOby)$_2$][PF$_6$]$_2$**, 0.1 M LiPF$_6$, and 0.5 M TBP).

***Table S5*. Photovoltaic performances of the DSSCs under AM1.5 illumination**[a]

dye	J_{SC} / mA cm^{-2}	V_{OC} / V	*ff*	PCE / %
LG4	10.3 (9.84 ± 0.6)	0.848 (0.845 ± 0.004)	0.778 (0.779 ± 0.002)	6.76 (6.48 ± 0.4)
LG4+XY1B	12.5 (11.9 ± 0.6)	0.877 (0.878 ± 0.001)	0.768 (0.770 ± 0.004)	8.40 (8.05 ± 0.4)

[a] Photovoltaic parameters deriving from the highest PCEs. The values in parentheses denote average values from three independent experiments. Error bars represent a standard error of the mean.

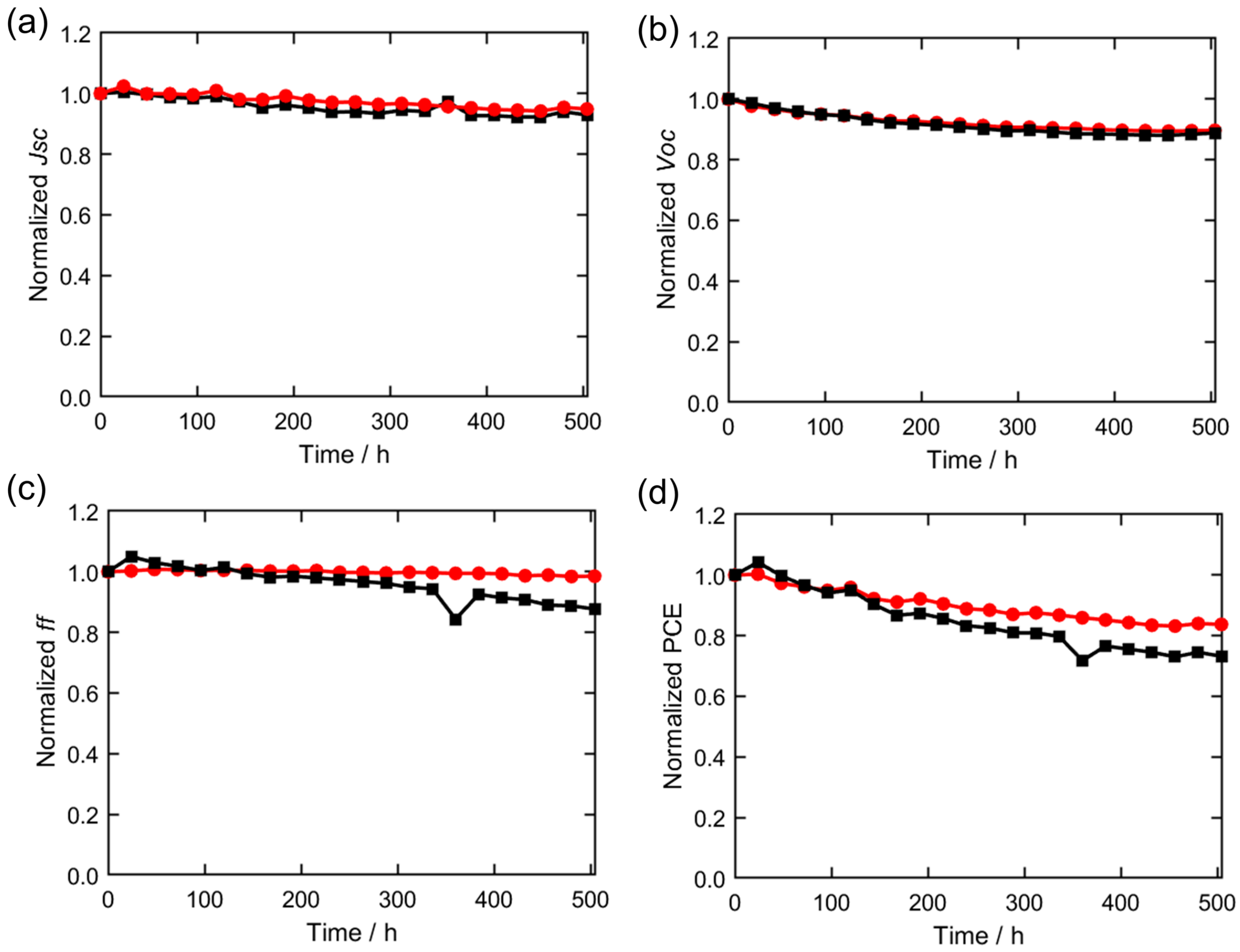

Figure S36. Variation of the normalized photovoltaic parameters (a) J_{SC}, (b) V_{OC}, (c) *ff*, and (d) PCE with aging time for the DSSCs with **FL1+XY1B** (red) and **LG4+XY1B** (black) using **[Cu(2MeOby)$_2$][PF$_6$]/[Cu(2MeOby)$_2$][PF$_6$]$_2$** redox shuttle (0.1 M **[Cu(2MeOby)$_2$][PF$_6$]**, 0.025 M **[Cu(2MeOby)$_2$][PF$_6$]$_2$**, 0.1 M LiPF$_6$, and 0.5 M TBP) measured under white-light illumination (100 mW cm^{-2}) at 25 °C for 500 h.

9. References

[S1] W. T. Yap and L. M. Doane, *Anal. Chem.*, 1982, **54**, 1437-1439.

[S2] M. J. Frisch, G. W. Trucks, H. B. Schlegel, G. E. Scuseria, M. A. Robb, J. R. Cheeseman, G. Scalmani, V. Barone, B. Mennucci, G. A. Petersson, H. Nakatsuji, M. Caricato, X. Li, H. P. Hratchian, A. F. Izmaylov, J. Bloino, G. Zheng, J. L. Sonnenberg, M. Hada, M. Ehara, K. Toyota, R. Fukuda, J. Hasegawa, M. Ishida, T. Nakajima, Y. Honda, O. Kitao, H. Nakai, T. Vreven, J. A. Montgomery, Jr., J. E. Peralta, F. Ogliaro, M. Bearpark, J. J. Heyd, E. Brothers, K. N. Kudin, V. N. Staroverov, T. Keith, R. Kobayashi, J. Normand, K. Raghavachari, A. Rendell, J. C. Burant, S. S. Iyengar, J. Tomasi, M. Cossi, N. Rega, J. M. Millam, M. Klene, J. E. Knox, J. B. Cross, V. Bakken, C. Adamo, J. Jaramillo, R. Gomperts, R. E. Stratmann, O. Yazyev, A. J. Austin, R. Cammi, C. Pomelli, J. W. Ochterski, R. L. Martin, K. Morokuma, V. G. Zakrzewski, G. A. Voth, P. Salvador, J. J. Dannenberg, S. Dapprich, A. D. Daniels, O. Farkas, J. B. Foresman, J. V. Ortiz, J. Cioslowski, and D. J. Fox, Gaussian 09, revision D.01; Gaussian, Inc.; Wallingford, CT, 2013.

[S3] S. Ito, T. N. Murakami, P. Comte, P. Liska, C. Grätzel, M. K. Nazeeruddin and M. Grätzel, *Thin Solid Films*, 2008, **516**, 4613-4619.

[S4] Y. Kurumisawa, T. Higashino, S. Nimura, Y. Tsuji, H. Iiyama and H. Imahori, *J. Am. Chem. Soc.*, 2019, **141**, 9910-9919.

[S5] J. Ding, M. Day, G. Robertson and J. Roovers, *Macromolecules*, 2002, **35**, 3474-3483.

[S6] A. Yella, H.-W. Lee, H. N. Tsao, C. Yi, A. K. Chandiran, M. K. Nazeeruddin, E. W.-G. Diau, C.-Y. Yeh, S. M. Zakeeruddin and M. Grätzel, *Science*, 2011, **334**, 629-634.

[S7] N. V. Krishna, J. V. S. Krishna, S. P. Singh, L. Giribabu, L. Han, I. Bedja, R. K. Gupta and A. Islam, *J. Phys. Chem. C*, 2017, **121**, 6464-6477.

[S8] G. Zhang, K. Tan, S. Xian, K. Xing, H. Sun, G. Hall, L. Li and J. Li, *Inorg. Chem.*, 2021, **60**, 11730-11738.

[S9] M. Karpacheva, F. J. Malzner, C. Wobill, A. Büttner, E. C. Constable and C. E. Housecroft, *Dyes and Pigments*, 2018, **156**, 410-416.

[S10] Y. Saygili, M. Söderberg, N. Pellet, F. Giordano, Y. Cao, A. B. Muñoz-García, S. M. Zakeeruddin, N. Vlachopoulos, M. Pavone, G. Boschloo, L. Kavan, J.-E. Moser, M. Grätzel, A. Hagfeldt and M. Freitag, *J. Am. Chem. Soc.*, 2016, **138**, 15087-15096.

[S11] L. Kavan, Y. Saygili, M. Freitag, S. M. Zakeeruddin, A. Hagfeldt and M. Grätzel, *Electrochim. Acta*, 2017, **227**, 194-202.

[S12] T. Higashino, H. Iiyama, I. Nishimura and H. Imahori, *Chem. Lett.*, 2020, **49**, 936-939.

[S13] P. Ferdowsi, Y. Saygili, S. M. Zakeeruddin, J. Mokhtari, M. Grätzel, A. Hagfeldt and L. Kavan, *Electrochim. Acta*, 2018, **265**, 194-201.